Contents lists available at ScienceDirect

Energy Conversion and Management

journal homepage: www.elsevier.com

Development of an artificial neural network based virtual sensing platform for the simultaneous prediction of emission-performance-stability parameters of a diesel engine operating in dual fuel mode with port injected methanol

Dipankar Kakati[a], Sumit Roy[b,*], Rahul Banerjee[a]

[a] Department of Mechanical Engineering, NIT Agartala, Tripura 799046, India
[b] Department of Mechanical Engineering, BML Munjal University, Gurgaon 122413, India

ARTICLE INFO

Keywords:
Diesel-methanol
Port fuel injection
Partially premixed combustion
Common rail diesel injection
Artificial neural network
Virtual sensing platform

ABSTRACT

The present work explores the potential of an artificial neural network platform to emulate the performance, emissions and stability indices of an existing single cylinder diesel engine operating in dual-fuel mode with methanol port injection under varying fuel injection pressure. This investigation is further augmented by hydrous methanol injection strategies. Brake power, fuel injection pressure, diesel specific fuel consumption, methanol specific fuel consumption, air flow rate, exhaust oxygen and temperature have been chosen as the model inputs while oxides of nitrogen, unburned hydrocarbon, carbon monoxide, carbon dioxide, soot have been chosen as the emission responses to be modelled along with equivalent brake specific fuel consumption as the performance response and coefficient of variance of indicated mean effective pressure as the stability parameter to be estimated. Absolute, relative and percentage-based statistical error metrics have been employed for model evaluation. The developed model shows an excellent agreement with the experimental data as evident from its extremely low normalized mean square error, symmetric mean absolute percentage error, Normalized root mean square error, mean squared relative error footprint coupled with high coefficient of determination which was observed to be within a range of 0.983–0.9999 and a corresponding Nash Sutcliffe coefficient of efficiency of 85%–99.6%. Furthermore, low Theil uncertainty evaluation and Kullback-Leibler Divergence values imparted a commendable credence of robustness to the estimation capability of the developed model. The present study manifests a computationally efficient and reliable virtual sensing platform to simultaneously emulate the emission-performance and stability parameters of a diesel-methanol partially premixed dual fuel operational paradigms in real time engine control strategies.

1. Introduction

With the ever-increasing challenges to comply with stricter emission mandates at every successive iteration of international legislations on one hand and the consumer need of better fuel economy on the other, have resulted in the emergence of innovative low temperature combustion (LTC) vectors such as homogeneous charge compression ignition (HCCI) [1], partially premixed compression ignition (PPCI) [2], premixed compression ignition (PCI) [3], premixed charge compression ignition (PCCI) [4], dual fuel reactivity-controlled compression ignition (RCCI) [5], thermally stratified compression ignition (TSCI) [6], spark assisted compression ignition (SACI) [7] in all its renditions over the last decade to keep the diesel contemporary to such expectations. The novelty and appeal of such emerging combustion concepts emanate from the possibility of harnessing the advantages posed by the difference of the ignition characteristics of the participating fuels in achieving the constrictive emission targets as well as significantly improving

Abbreviations: ANN, artificial neural network; BDO, baseline diesel operation; BSFCeq, equivalent brake specific fuel consumption; CRDI, common rail direct injection; DAQ, data acquisition; ECU, engine control unit; EGR, exhaust gas recirculation; FIP, fuel injection pressure; GUI, Graphical user interface; HIL, hardware-in-the-loop; KL, Kullback-Leibler divergence; MSRE, mean squared relative error; MAPE, mean absolute percentage error; NOx, oxides of nitrogen; NMSE, normalized mean square error; NRMSE, normalized root mean square error; NSCE, Nash-Sutcliffe coefficient of efficiency; OBD, onboard diagnostic; PFI, port fuel injection; ppm, parts per million; R, coefficient of correlation; R^2, coefficient of determination; RCCI, reactivity controlled compression ignition; RI, ringing intensity; RMSE, root mean square error; RTD, resistance thermocouple diode; SIT, system identification tool; SMAPE, symmetric mean absolute percentage error; VCR, variable compression ratio.

* Corresponding author.
Email address: sumitroy@hotmail.de (S. Roy)

https://doi.org/10.1016/j.enconman.2019.01.087
Received 24 September 2018; Accepted 22 January 2019
Available online xxx
0196-8904/

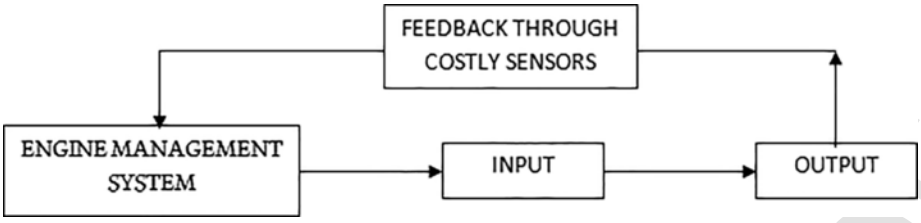

Fig. 1. Conventional engine management process.

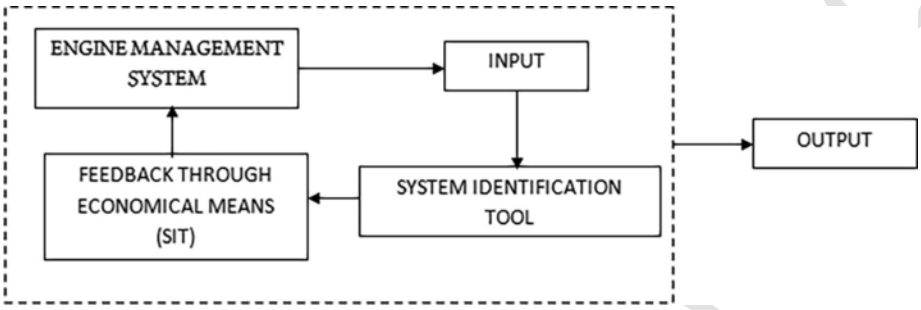

Fig. 2. Engine management process with SIT.

Table 1
Experimental engine details.

Parameter	Specification
Engine details	Kirloskar TV1 (Single cylinder, four-stroke diesel, water cooled, compression ignition)
Bore and stroke	87.5 × 110 mm
Compression ratio	17.5:1
Rated output	3.5 kW@1500 rpm
dynamometer	Eddy current loading unit, 0–12 kg
Fuel Injection timing	23° BTDC
Connecting rod length (mm)	234
Crank radius (mm)	55
Max. brake mean effective pressure @1500 rpm	6.374 bar
Fuel injection	Direct injection
Fuel injection system	Pump in line nozzle injection
Needle lift (mm)	0.25
Piston bowl	Hemispherical
Governing	Class B1 as per is 10,000 (Part 7) 1989
Swept volume	661.5 cc
Dynamometer arm length	185 mm

fuel economy simultaneously. The fact that existing conventional fuels can be utilized along with alternative fuels in existing engine configurations have added an index of sustainability to the impetus to such developments in engine research as no radical design shifts are necessary albeit invoking new operational methods. Work of Liu et al. [8] has unanimously yielded the significant superiority of such diesel-alcohol LTC techniques in addressing the omnipresent emission-performance trade-off characteristics of conventional diesel engine operation and also to that of standard dual fuel modes. That said, the incentives of such combustion modes are critically contingent on optimal control and actuation of several operating variables to ensure proper combustion phasing of the fuels differing in their cetane-octane ratings in an engine cycle [9]. Such precision in control in turn necessitates robust engine management systems EMS. Contrary to conventional look-up table-based EMS strategies, the complexities of control in such evolving combustion strategies demand accurate and dynamic estimation of the system non-linearity on-the-fly [10]. As a result, on-board diagnostic capability and the ability to control in real time [11] has become increasingly pertinent in rationalizing the distinct advantages of such emerging combustion methodologies which are having a significantly higher dimension of parametric degrees of freedom that need to be addressed simultaneously. Compared to the explicit multi-physics based computational fluid dynamic platforms generally employed for a high-fidelity system characterization of such diesel combustion modes, artificial neural network-based engine system identification strategies offer a pragmatic alternative for real time deployment in engine management systems geared towards realizing the high level of responsiveness necessitated for controlling the premixed diesel combustion modes [12]. Conventional engine management process and SIT based engine management process are depicted in Figs. 1 and 2 respectively.

Congruent to global initiatives on attempts to shift to sustainable bio-resource based fuels methanol premixed advanced diesel combustion concepts have garnered an increasing interest in contemporary engine research on account of its ability to significantly reduce regulated emissions simultaneously, [13] coupled with the possibility of increased diesel fuel economy at high methanol energy share ratios [14] over a wide span of desired engine operational loads. The fact that such partially premixed combustion concepts provide a proven ability to accommodate conventional and alternative fuels at unprecedented levels of effectiveness hitherto unattainable in standard DDF modes, create a sustained potential in future diesel engine research. The advantages of such methanol based PPCI strategies notwithstanding, studies [15] dedicated to such exploration distinctly outline the sensitivity of the engine emission, thermal efficiency and stability indices on the variation of the parameters involved in ascertaining the optimal PPCI mode of operation. This is indicative of the pivotal need to characterize the operational design space for any subsequent optimization endeavour to meet emission-performance trade-off targets set. Literature examination [16] to this effect reveals an extensive use of chemistry coupled multi-physics based CFD strategies to emulate system behavior with high fidelity for methanol-diesel PPCI modes validated against actual experimental results. However, such CFD based SIT endeavors entail a computational footprint which deters any consideration of its virtues in real time decision making applications especially in case of its deployment as a virtual sensing platform. It is to this end that the present study establishes itself as an alternative SIT platform for such methanol-based diesel PPCI operations, the observed accuracy and robustness of which claim due consideration in its ready applicability in OBD based virtual sensing of the emission performance and stability parameters in real time [17] for onboard as well as in hardware-in-the-loop (HIL) explorations [18] or even as a CFD co-solver to reduce the

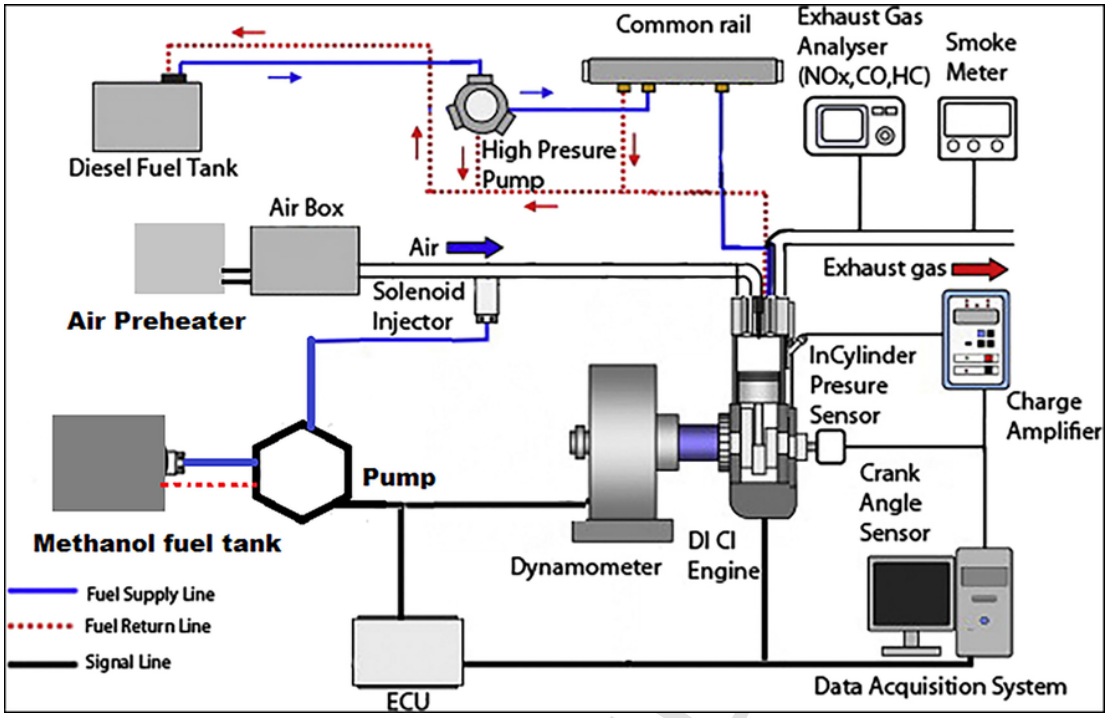

Fig. 3. Schematic diagram of experimental setup.

Table 2
Chronology of the experimental process.

Sweep →

Sweep ↓	50% load		75% load		100% load	
4 ms	400 bar		4 ms	400 bar	4 ms	400 bar
	500 bar			500 bar		500 bar
	600 bar			600 bar		600 bar
6 ms	400 bar		6 ms	400 bar	6 ms	400 bar
	500 bar			500 bar		500 bar
	600 bar			600 bar		600 bar
8 ms	400 bar		8 ms	400 bar	8 ms	400 bar
	500 bar			500 bar		500 bar
	600 bar			600 bar		600 bar
10 ms	400 bar		10 ms	400 bar	10 ms	400 bar
	500 bar			500 bar		500 bar
	600 bar			600 bar		600 bar

Table 3
Technical details of CRDI System.

Specification	Resources
Type	Common Rail Injection System
Make	Bosch
Injection Pressure	10–120 MPa
Number of Holes	5 (Symmetric)
Nozzle Diameter	0.15 mm
Injection Angle	1200
Fuel Injection Timing	23°BTDC (static)

Table 4
Types of test cycles for different engines.

Type of test cycles	Type of engines
Type C	Off-road vehicles and industrial equipments
Type D	Constant speed
Type E	Marine applications
Type F	Rail traction
Type G	Utility, lawn and garden; typically < 20 kW
Type H	Snowmobile

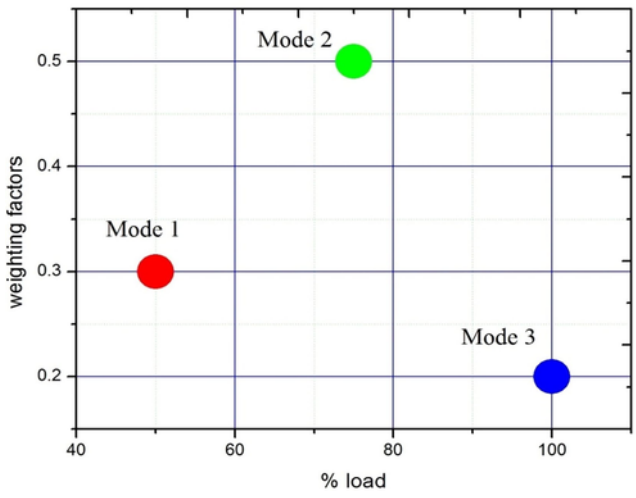

Fig. 4. Weighting factors for different mode of operations.

computational cost of detailed reaction mechanism routines [19] in such methanol-diesel PPCI explorations.

IC engine paradigms have extensively exploited such inherent advantages of ANN strategies to characterize both SI and CI engine responses. In SI engines, ANN approach has been used to predict performance, emissions [20], air–fuel ratio control [21] and variable valve lift and timing [22] while in diesel engines emission-performance [23] as well as particulate matters [24] have been forecasted utilizing ANN platform. Canakci et al. [25] have utilized ANN platform for system identification of an existing diesel engine operating with the waste frying oil biodiesel under varying engine speed at full load condition. In their study, it was observed that ANN was capable of identifying the complex correlations of fuel properties with engine emission and performance for different blends of biodiesel. Oguz et al. [26] have stud-

Table 5
Percentage uncertainty of each instrument involved in measurement.

Experimental instrumentation	Make type	% Uncertainty of sampling
Dynamometer (integrated speed sensing unit)	Eddy Current Type-Model AG10 of Saj Test Plant Pvt. Ltd.	±1
Load sensor	Make Sensotronics Sanmar Ltd., Model 60001	±0.2
Load indicator	Make Selectron, model PIC152-B2	±0.1
Fuel measuring unit	Make Apex-Model:FF0.012	±1.5
Fuel flow transmitter	Differential pressure transmitter; Make Yokogawa-Model EJA110-EMS-5A-92NN	±0.065
Cylinder pressure sensor	Piezo-sensor of Make PCB Piezotronics Inc., ModelHSM111A22	±0.1
Fuel injector pressure sensor	Piezo-sensor; Make: PCB Piezotronics Inc, Model-M108A02	±0.15
Crank angle sensor	Make Kubler-Germany Model 8.3700.1321.0360	±0.2
Temperature sensor	Make Radix; Type RTD, PT100 and Thermocouple Type K	±0.4
Temperature transmitter	Make Wika, model T19.10.3K0-4NK-Z	±0.2
Air flow transmitter	Make-Wika;Model-SL1	±0.5
Rotameter	Eureka make, cooling water 40–400 lph	±2
Exhaust gas analyzer	AVL(India)Model:444–5 gas analyzer fitted with Di-gas sampler	
1.Carbon monoxide (CO)		<0.6% vol ± 0.2 ≥0.6% vol ± 0.3
2.Carbon dioxide (CO2)		<10% vol ± 0.15 ≥10%vol ± 0.2
3.Total unburnt hydro carbons (TUHC)		<200 ppm vol ± 0.1 ≥200 ppm vol ± 0.2
4.Oxygen(O2)		<2% vol ± 0.2 ≥2% vol ± 0.3
5.Nitric oxide (NOx)		<500 ppm vol ± 0.2 ≥500 ppm vol ± 0.9
6. Smoke (Opacity)	AVL 437 smokemeter	1

ied the effects of bio fuels on diesel engine performance by employing ANN approach for prediction of torque, power, fuel consumption and specific fuel consumption. The experimental and the ANN estimated values were found to be in good correlation establishing through very small and negligible deviations between them. As established from the statistical regression analysis with reliability value of 99.94% ($p = 0.9994$ and $p > 0.05$) in their study, ANN modelling is proven to be an accurate and appropriate method for estimation of diesel engine performance. Further in the study of Ghobadian et al. [27], ANN approach was found to be a reliable, simple and accurate in predicting the performance of the diesel engine parameters and compared to other numerical and mathematical methods, ANN is more desirable due to its inherent robustness while encountering complex multivariate nature of the problem. While Hashemi et al. [28] in their study have utilized the ANN platform as a prediction method for estimating the emission components of NOx, CO, CO2 and HC from heavy-duty diesel vehicles by varying input variables of torque, speed, their first and second derivative in various time steps along with two new variables characterizing speed variability over 150 s. In their study of heavy duty engines, the collection of data had been carried out from an off-cycle Urban Dynamometer Driving Schedule (UDDS). Their study has showed the artificial neural network as an appropriate technique for simulating complex correlations of different parameters and emissions and thus provides the opportunity to emulate real time emissions of a heavy-duty engine run over a highway route.

1.1. Motivation of the present study

Off-line engine system characterization based on data driven artificial intelligence platforms possess a great potential [29] for developing a very fast [30], adaptive and robust multidimensional model of the engine performance and emission behavior in a chosen parametric design space. Furthermore in the work of Rai et al. [31], such strategies of artificial intelligence have been appreciated compared to traditional parametric regression techniques (ex: Response Surface Modeling), for accommodating data with considerable degrees of uncertainties of observation. The intrinsic capability of an artificial neural network system for adapting to highly nonlinear behavior of the system variables as is evident in the genesis of typical engine emissions have substantiated itself as a robust and acclaimed system identification tool [32] in the realm of engine control systems.

Besides, it's innate parallel solver architecture and its independence from the underlying physics of the correlation of the participating variables under study albeit its "black box" tag provides it with the significant advantage of obtaining model response at high computational speeds even when offered with noisy, partial or incomplete set of data [17], thereby reducing EMS decision response time window considerably for efficient control. The potential advantages of ANN based models coupled with its computational economy and the ease of integration in engine OBD systems provide a compelling basis of exploiting its virtues as a virtual sensing system for continuous on-board estimation of regulated emissions in real time [26,28] the option of measurements of which by actual sensors do not exist or are obviated by the perspectives of cost and practicality.

Furthermore, ANN modeling being essentially data driven is susceptible to the inherent pitfalls of overfitting of system responses when presented with operational data beyond its training range. Hence the

Table 6
Total measurement uncertainty of each parameter.

Computed performance parameter	Measured variables	Instruments used	% uncertainty of measuring instrument	calculation	Total % uncertainty
BP	Load, rpm	Load sensor, load indicator, speed measuring unit	0.2, 0.1, 1	$\sqrt{(0.2)^2 + (0.1)^2 + (1)^2}$	1.02
Load	load	Load sensor, load indicator	0.2, 0.1	$\sqrt{(0.2)^2 + (0.1)^2}$	0.22
Fuel flow	Fuel flow	Fuel measuring unit and fuel flow transmitter	0.065, 1.5	$\sqrt{(0.065)^2 + (1.5)^2}$	1.5
IMEP	Pressure, speed	pressure sensor, speed measuring unit	0.1, 1	$\sqrt{(0.2)^2 + (2)^2}$	1.005
EGT	Temperature	Temperature sensor, Temperature transmitter, indicator	0.4, 0.2, 0.1	$\sqrt{(0.4)^2 + (0.2)^2 + (0.1)^2}$	0.46
BSFC	SFC (diesel), BP	Fuel measuring unit, fuel flow transmitter, load sensor, load indicator, speed measuring unit	0.065, 1.5, 0.2, 0.1, 1	$\sqrt{(0.065)^2 + (1.5)^2 + (0.2)^2 + (0.1)^2 + (1)^2}$	1.82

Table 7
Details of GEP model parameters.

P_1	Function set	+,−,*,/, Sqrt, x^2, Exp, Ln, Inv Log, Pow, cube root, Min2, Max2, Avg2, Atan, Tanh, NOT (1-x).
P_2	Chromosomes	30
P_3	Head size	8
P_4	Number of genes	3
P_5	Linking function	addition
P_6	Mutation rate	0.044
P_7	Inverse rate	0.1
P_8	One-point recombination rate	0.3
P_9	two-point recombination rate	0.3
P_{10}	Gene recombination rate	0.1
P_{11}	Gene transportation rate	0.1

robustness of such models needs to be investigated prior to deployment for real time forecasting. The versatility of ANN in emulating the complexities of emission-performance responses in dual fuel mode of diesel–natural gas [33], diesel-hydrogen [12] as well as diesel-LPG [34] have already been extensively appreciated. However, examination of similar studies exploiting ANN method to emulate emission and performance responses in a diesel dual fuel environment yield little or no attention devoted to the necessities of invoking appropriate error or model uncertainty metrics to rationalize the robustness of the proposed models thereby undermining its potential applicability. In majority of the studies so highlighted, model accuracy evaluation has been principally biased on statistical metrics of Correlation Coefficient 'r' and Co-Efficient of Determination R^2 which is fundamentally limited in its sensitivity to the additive and proportional differences between the observed and predicted values [35] over the domain of interest. Thus, high r and R^2 scores in a high dimension parametric design space can be an elusive metric to claim model credibility as the latent variability of the responses with regard to the chosen input parameters remain unaccounted. Moreover the study of Armstrong et al. [36] dedicated to the cause of ascertaining appropriate metrics of model performance have concluded that sole reliance on such mean square error-based evaluation metrics are unsuitable for model appreciation especially when the modelling endeavour involves simultaneous emulation of data across different scales, a situation typically reflected in ANN based engine emission-performance meta modelling strategies. In view of the limitations outlined above, the present study is motivated to assess ANN model integrity through a comprehensive array of more credible error metrics corresponding to each of the respective categories of the prevalent statistical metrics. The ANN modelling being data driven technique, model responses is critically dependent upon the experimental data presented to it. To this end, to rationalize the uncertainty of the proposed ANN model, a detailed exposition on the instrument and sampling uncertainty of experimental data has been undertaken to estimate the individual variability of the model responses. The present study further incorporates distinct statistical metrics to quantify the forecasting uncertainties arising from randomness in weight initialization and data portioning (training and validation) during model development and tuning. The present modelling endeavour, however, has taken cognizance of the imperative need of taking the issue of engine stability under such methanol-diesel operation modes by incorporating COV_{IMEP} as a system response to be estimated simultaneously along with the emission-performance parameters of interest. Such considerations stem from the findings in the study of [37] focused on engine system characterization of similar diesel-methanol PPCI investigations. Thus, the study presents a first-of-a-kind *meta*-modeling endeavour to establish a credible and robust virtual sensing platform to characterize emission-performance and stability parameters simultaneously in methanol-diesel PPCI realms for real time forecasting and EMS decision making.

2. Materials and methods

The experimental study was carried out on an existing single cylinder four stroke variable compression ratio (VCR) CI engine of Kirloskar TV1 make as enlisted in Table 1 conforming to IS: 11170–1985. A water-cooled eddy current dynamometer of Saj Test Plant make model AG10 was coupled to the engine with an integrated speed sensing unit. The engine was factory set to run at a constant rpm of 1500 within an operational variability of ±30 rpm. The speed scanning interval of the dynamometer was set to 2000 ms to smoothen undesirable signal fluctuations. For sensing the load on the engine, a VPG Sensotronics make strain gauge type load sensor of a range of 0–50 kg has been integrated empowered with a load step sensitivity of ±0.1 kg.

The schematic diagram of the experimental set up has been shown in the Fig. 3. The instrumentation was interfaced to a computer through a DAQ Factory ® based DASTEP8 ® empowered with 16 MHz sampling frequency data acquisition platform synchronized with a crank angle encoder onto a GUI based Engine Combustion Analysis ® post processing software. The sampling frequency of DASTEP8 ensured a credible and robust anti-aliasing data acquisition platform by conforming to the Nyquist–Shannon Sampling Theorem as the DAQ sampling frequency capability was much higher than twice the highest frequency of 9600 Hz of the engine signal rate that was expected to be encountered during experimentation at a constant rpm of 1500. The DAQ routine was programmed to acquire in-cylinder and fuel injection pressure data at 1° crank interval and present the data smoothened over 100 consecutive cycles to compensate for cyclic variations at a particular load step of experimentation. Cylinder pressure was captured with a Piezo-sensor of Make PCB Piezotronics Inc. Model no. HSM111A22 engaged with a sampling uncertainty of ±0.1%. For taking measurement of cooling water temperature, a Radix make RTD type thermometer pt100 ranging from −200 °C to 500 °C with accuracy ±0.1 K was employed whereas the temperature of exhaust gases was measured using a K type thermocouple ranging from −180 °C to 1300 °C with accuracy of ±2.5 K. Additionally, the set up was equipped with a Rotameter of Eu-

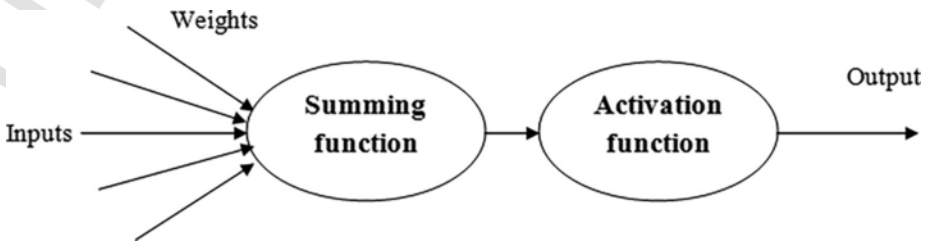

Fig. 5. Structure of an artificial neuron.

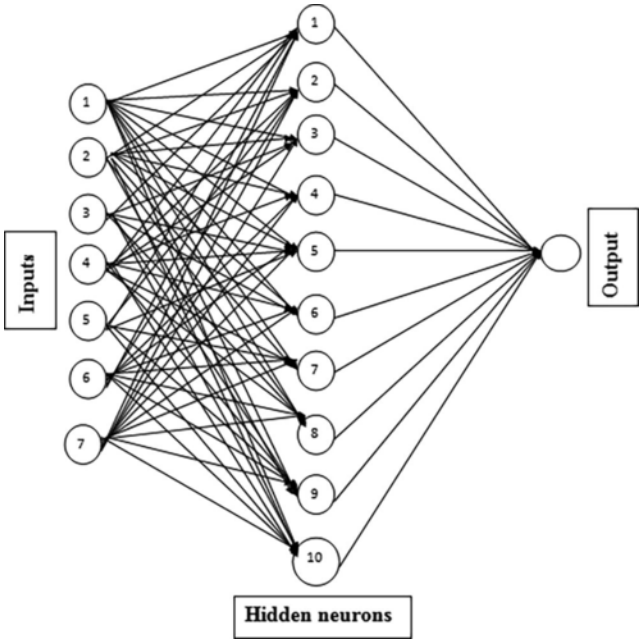

Fig. 6. Architecture of proposed ANN.

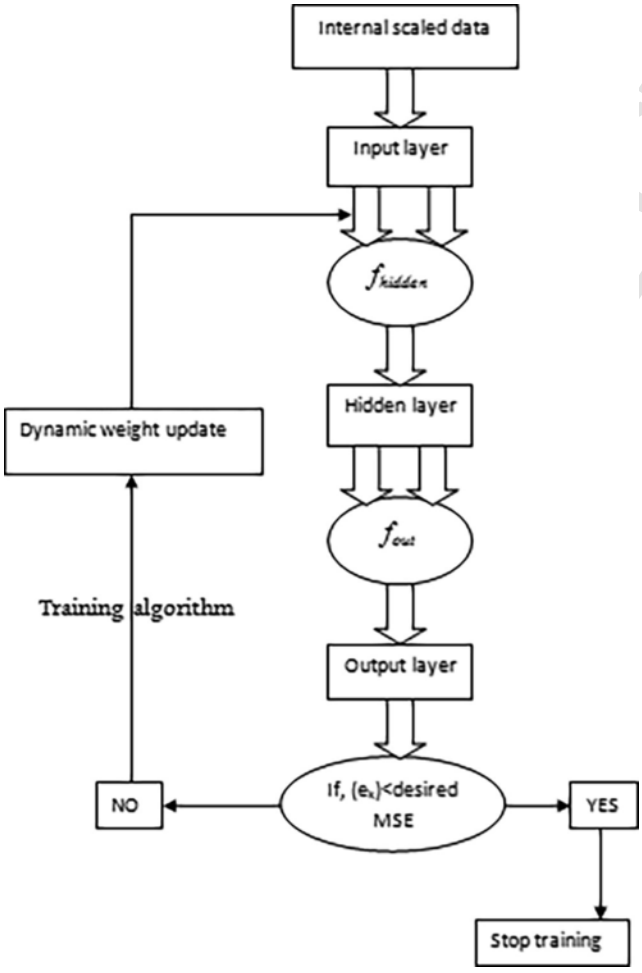

Fig. 7. Flow chart of iteration process.

reka make ranging from 40 to 400 L per hr. cooling water for measuring the water flow. The air box consisted of an M S fabricated orifice meter and manometer and the measurement was taken from the manometric depression. The consumption of diesel was calculated by the head difference of the burette of 12.4 mm diameter for a time period of 60 s.

Initially, the experimental engine was started with diesel only mode at no load condition which was continued for a certain period of time. For this present study, the operational mode was considered as 50%, 75% and 100% of full load conforming to ISO-8178. At each load, fuel injection pressure was varied from 400 to 600 bars as stated in Table 2 through a dedicated CRDI as detailed in Table 3 with a gradual increment of 100 bar. At all 50% load cases methanol PFI strategies could only be carried out to a maximum of 8 ms of injection duration beyond which data acquisition was impaired by engine instability issues arising out of intermittent misfires and engine vibrations. Proceeding forward, the load was gradually swept from 50% to75% and 100% of full load. For each load, the experimental sweeping sequence has been shown in the Table2 for entire scope of operation. All the data were recorded after achieving stable steady state condition at each step of experimentation.

For dual-fuel combustion mode, some additional arrangements were done in the existing system as shown in the Fig. 3. The existing inlet manifold was modified to incorporate methanol injector. The methanol injector was installed on manifold at a distance of 180 mm from the port. For avoiding wall impingement of methanol droplets, the inclination of the injector was kept at 45° with the inlet manifold. The whole methanol injection system is an independent system integrated with the existing engine set up synchronized with crank angle encoder. The Performance electronics USA make ECU of model no. PE3-SP000 was used in connection with the methanol injection. The fuel pump (model Bosch 0580454140) operating between 45 and 60 PSI was activated by a battery supplying electrical power at 12 V DC. The injector assembly model used in methanol injection was 15710M797D0 which was controlled by the ECU and actuated by the electrical pulses. The amount of methanol goes into the manifold depends on the time (millisecond or ms) for what the injector is kept open. However, the minimum pulse width for opening an injector defines the lower limit for the injection duration or pulse width. The typical values of opening time for any saturated injectors are 1 to 1.8 ms. Therefore, to compensate this difficulty the minimum initial main injection duration was set to 4 ms in this study.

. The inlet temperature for all methanol strategies was maintained above 64.7 °C to ensure complete evaporation of methanol before cylinder induction. The methanol was injected at crank angle of exhaust valve closing (5° ATDC) for avoiding any escape of gaseous methanol during inlet and exhaust valve overlap in the engine cycle. The pilot fuel was injected at 23°CA BTDC. Depending on the load, PID controls the amount of diesel fuel to be injected to keep the engine rpm constant. As methanol percentage increases in the combustion, diesel fuel quantity automatically drops to run the engine at constant 1500 ± 30 rpm. The engine performance and emissions characteristics were captured using different necessary instruments and their uncertainty in measuring performance and emissions have been reported in total sampling uncertainty. Emissions of NOx, O_2, lambda, HC and CO were recorded using a 5 Gas analyzer (AVL Di-Gas 444) and smoke is measured using AVL 437 smoke-meter whereas the soot is calculated from FSN using the formula shown below

$$soot(mg/m^3) = \frac{1}{0.405} \times 4.95 \times FSN \times \exp(0.38 \times FSN) \quad (1)$$

In this experimental endeavor, the operational modes were considered according to ISO-8178 (D1). The off-road engines have a wide variety in power outputs as well as configuration compared to on-road

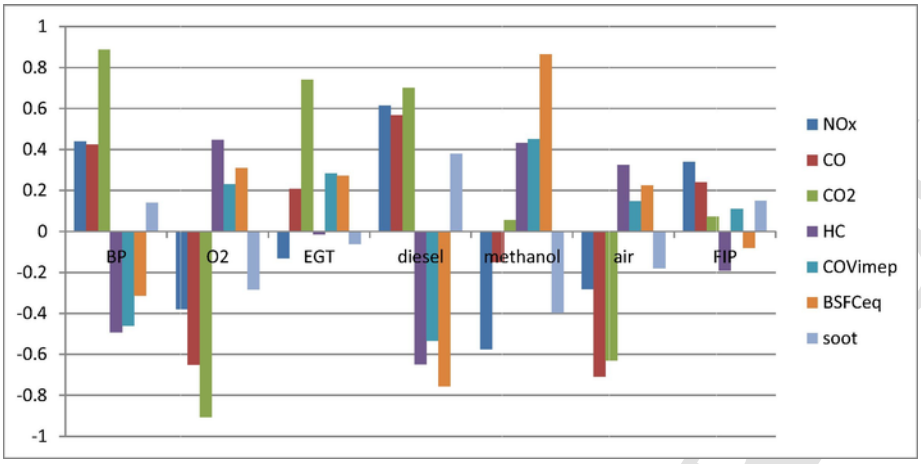

Fig. 8. Effects of input variables on desired outputs as per their Pearson's correlation.

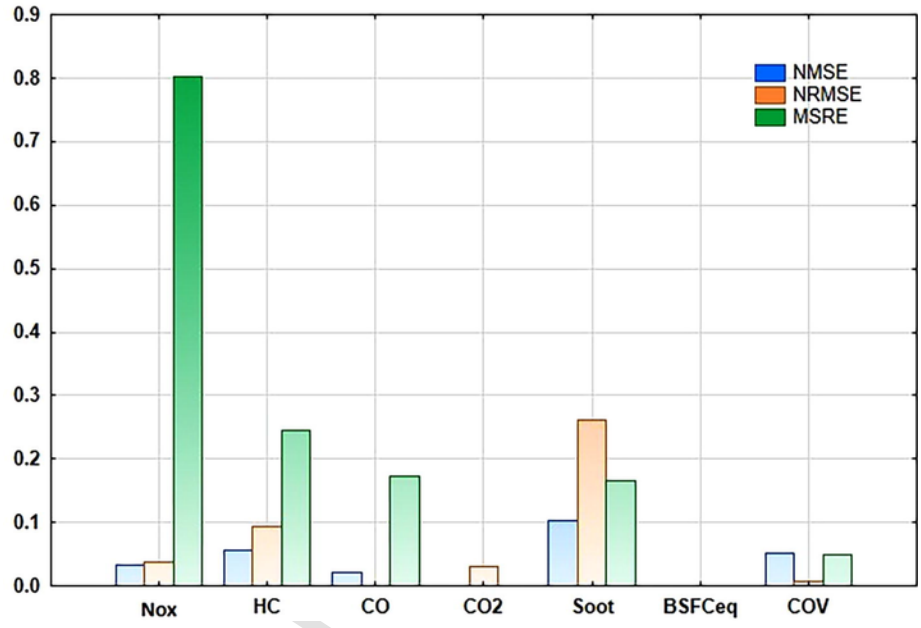

Fig. 9. Comparison of relative errors of the model for 6 neurons.

application engines. ISO-8178 trimmed down the bulky test procedures for off-road engines with the intention of simplifying the certification of off-road engines. The ISO 8178 includes a collection of steady-state engine dynamometer test cycles (designated as type C1, C2, D1, D2 etc.) with different weighting factors designed for different classes of engines and equipment. In this experimentation 50%, 75% and 100% of full-load has been considered as mentioned in ISO-8178 for D1 (3-mode test cycle) type of engines (Table 4). Operating modes and weighting factors of type D engines according to ISO-8178 test cycles [38] is shown in the Fig. 4. Contingent to initial data analysis of the emission-performance-stability output parameters under consideration in the present study, it was evident that anhydrous methanol-diesel operation at 75% full load yielded the best trade-off vantage for furthering the cause of exploring the effect of hydrous methanol-diesel strategies. It was to this end, that 10% and 30% hydrous methanol injection strategies were additional examined at that load. Engine instability experienced beyond 30% hydrous-methanol at the chosen load deterred any study of the effect of higher percentages of water content in the PFI methanol–water solution. The choice of hydrous methanol at 75% load was further motivated by the dictates of the ISO 8178 D (I) test mode which imparted the highest weighting factor to engine operation at the, 75% load point consequentially demanding its relevant importance for exploring further experimental strategies in complement to baseline engine system characterization endeavors.

The ANN modelling technique being data driven, model response is critically dependent upon the experimental data presented to it. Reiterating the considerations of the necessity to sustain a credible index of generalization capability of such a data driven metamodel, it was deemed pivotal that the variability of the experimental data set presented to the ANN solverfor training was ascertained in prior to estimate the individual variability of the model responses. To this end, a comprehensive instrumentation and sampling uncertainty analysis affecting the experimental data was undertaken in line with the methods outlined in the study of [39] and reported in detail in Tables 5, 6 and 8 for ready reference.

3. Artificial neural network modeling

ANN is a black box type of artificial system which consists of processing elements and many interconnections. It does not require any rigorous information of the problem under study; rather it can acquire the knowledge from the existing data through learning process. As de-

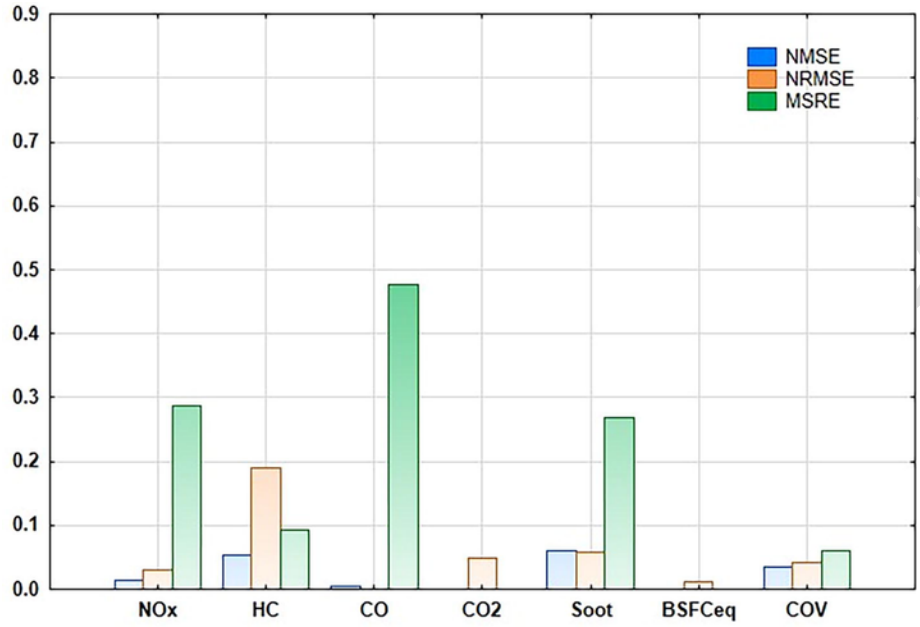

Fig. 10. Comparison of relative errors of the model for 8 neurons.

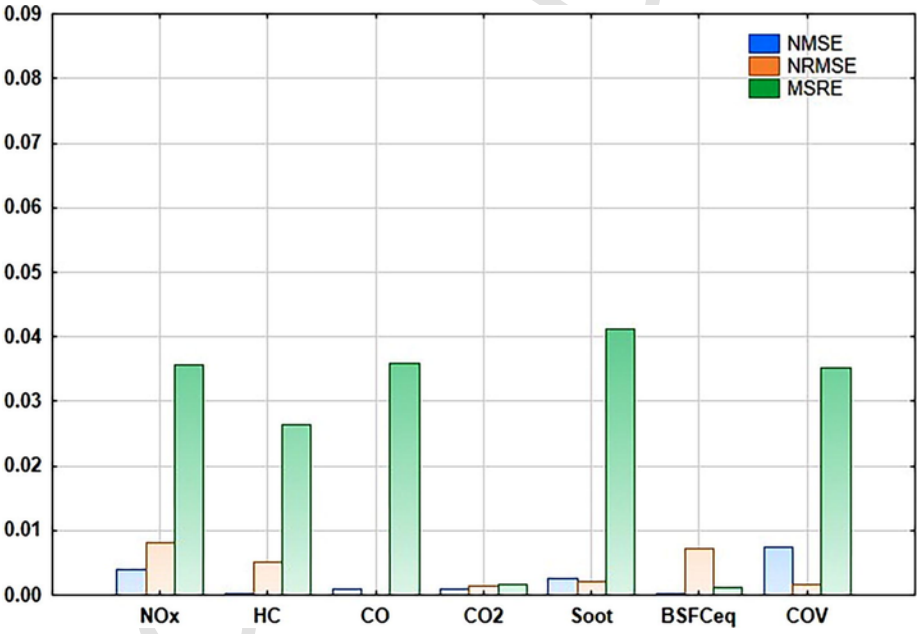

Fig. 11. Comparison of relative errors of the model for 10 neurons.

picted in the Fig. 5, an artificial neuron has mainly five parts inputs, weights, sum function, activation function and outputs. A training process in ANN modeling usually contains construction of network, feed forward method and back propagation method [12]. Depending on the strength of inputs, the output of each neuron is calculated by feed forward method. Whereas in back propagation method, network weights are updated to improve the performance of the model based on minimizing mean square error (MSE). The network performance is improved by adjusting the weights through several iterations in the training program.

A typical ANN model contains input layer, output layer and single or multiple hidden layers (Fig. 6). ANN iteration process flowchart is depicted in Fig. 7 [12]. MATLAB® neural network toolbox has been utilized in this present case as the ANN iteration solver in line with the study of Noor et al. [40]. In this study, total 66 numbers of non-repeated data sets were available which had been acquired experimentally whereas it was perceived from the study of Roy et al. [33] that the data sets were divided randomly in three parts out of which 70% were selected for training the network and other 30% were divided in two equal halves for validation and testing of the trained network. Hence subsequently in this case, 46 numbers (70%) of dataset were selected randomly for training purpose followed by 10 numbers of dataset (15%) for cross validation and 10 numbers of dataset for testing the performance of the developed model.

It is of extreme importance to apply a proper training rule which helps the activation function to estimate the desired outputs through internal adjustment of network weights. A training rule is a procedure in which the weights and biases of a network are adjusted and the error function between the network inputs and outputs are minimized. For this study, an advanced training algorithm called Levenberg-Mar-

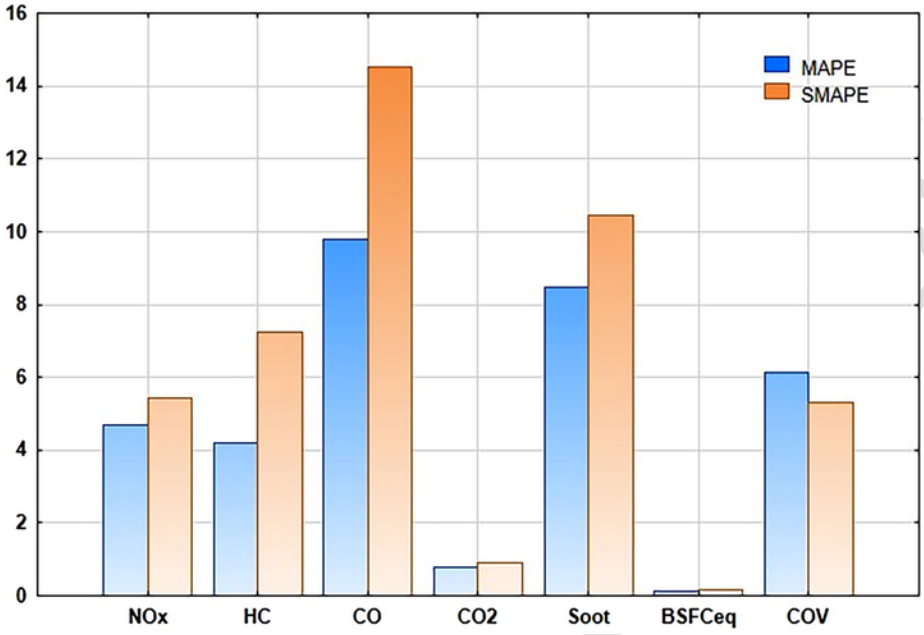

Fig. 12. Comparison of percentage based errors of the model for 6 neurons.

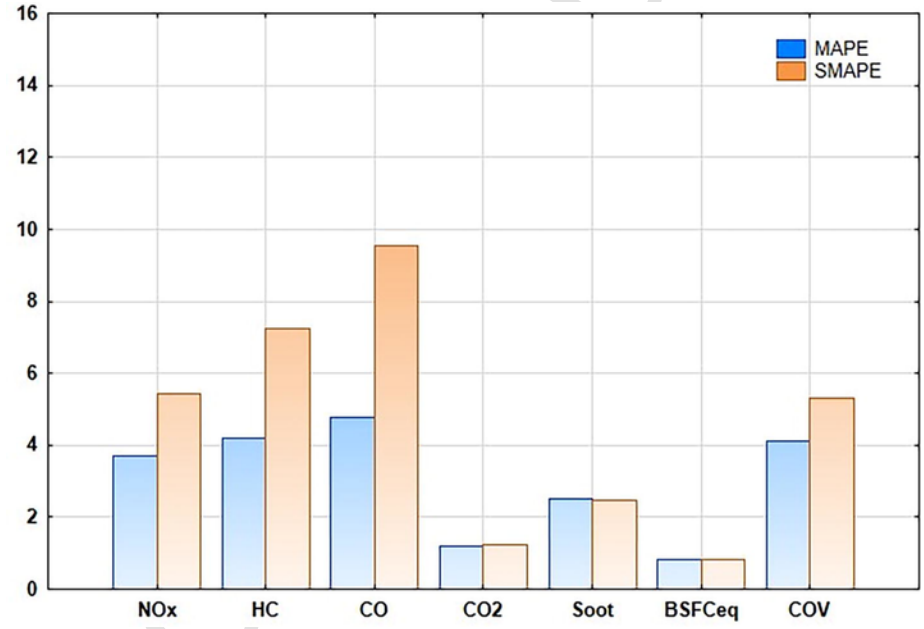

Fig. 13. Comparison of percentage based errors of the model for 8 neurons.

quardt back propagation method was used for training and learning process due to its fast converging nature [12]. Levenberg-Marquardt is a hybrid method which combines the steepest descent and Gauss-Newton method to produce a more efficient technique for faster convergence. It incorporates a second order derivative for error minimization resulting in a faster solution. A well-established easily differentiable Log-sigmoid activation function was used in this study [33] for both hidden and output layers. The inputs and outputs have been scaled through logistic sigmoid transfer function. For this study, Mean Square Error (MSE) was set as the loss function to be minimized by the learning algorithm.

In this present case of study, the considered input and output variables being differently scaled required a normalization endeavour to standardize the training data set across the variables of interest. Though several methods exist to this end, the Min-Max strategy Fig. 6 was adopted for its ability to preserve the relationships among the variables in the original dataset without loss of generalization [41]. Furthermore, in contrast to the prevalent practice of a Min-Max standardization range of 0–1, the present study has adopted a corresponding range of 0.1–0.9 in order to avoid saturation of the sigmoid transfer function of the hidden and output neurons [42] during model training (Eq. (2)). These are the saturation regions where the gradient/derivative is too small which slows down the learning process by increasing the weight up gradation time of the network at each iteration.

$$y = 0.1 + 0.8 \times \frac{x - x_{\min}}{x_{\max} - x_{\min}} \tag{2}$$

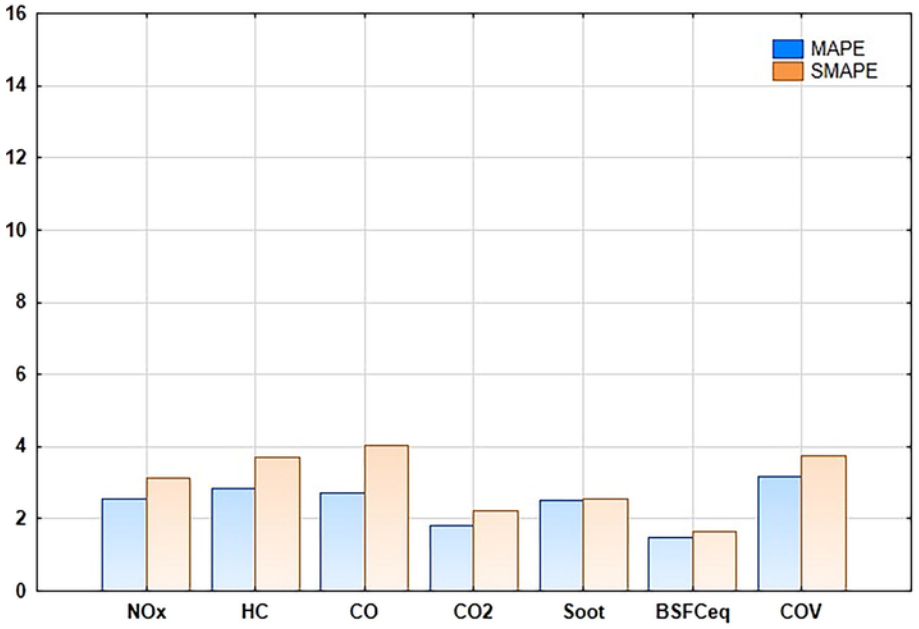

Fig. 14. Comparison of percentage based errors of the model for 10 neurons.

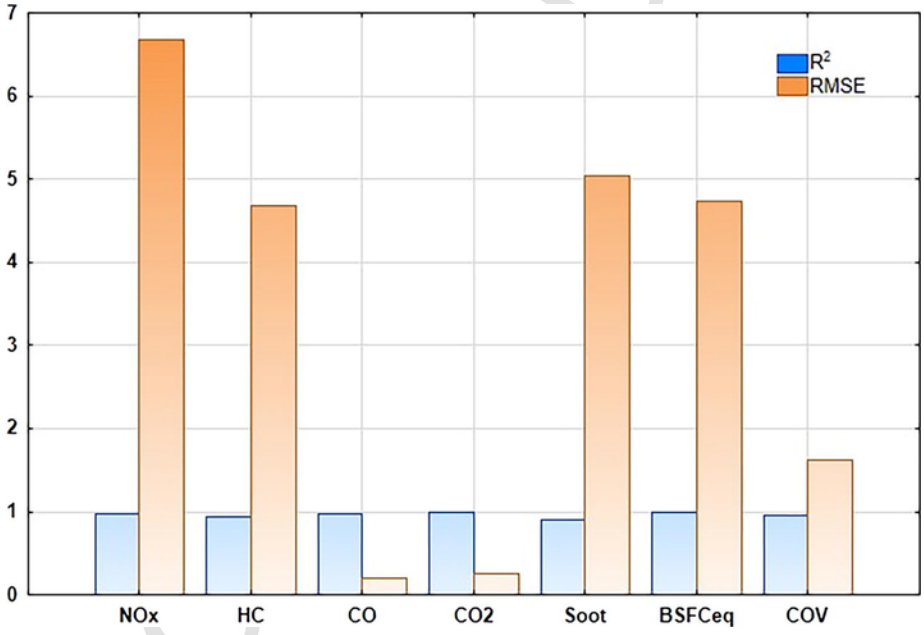

Fig. 15. Comparison of the correlation coefficient metrics for 6 neurons.

where, y is the normalized value, x_{max} is the maximum value and x_{min} is the minimum value while x is the absolute value of the data set.

3.1. Choice of input and output variables

Accomplishment of success of an ANN model highly depends on the clear understanding of the situation under study and the selection of the most significant input variables. In this study of diesel-methanol PPCI modeling, considering the degree of influence of the control parameters on the response parameters, the variables have been opted for characterization of the design space. Diesel, methanol and air flow rates have been considered as inputs in this study which represents the available fuel and oxygen in the combustion chamber. Brake power (BP) and fuel injection pressure (FIP) are two other important input variables that have been incorporated by considering their significant influences on emission and performance parameters as depicted in Fig. 8. AL-Shemmeri et al. [43] in their study have observed a strong correlation between the flame temperature and the formation of NOx and hence the Exhaust gas temperature a subset of in-cylinder temperature has been chosen as an input variable for modeling in this study. Intending to reduce complexity of the model, introduction of output oxygen is also considered as an additional input which reflects the Brett Schneider lambda [44] directly which is an independent element of the combustion that occurs inside the cylinder. In this present study NOx, CO, CO_2, HC and soot as emission parameters, BSFCeq as performance and additionally COV_{IMEP} as combustion parameter for stability analysis have been considered as output variables. As the methanol input content and amount of water content was inherently co-related for a given

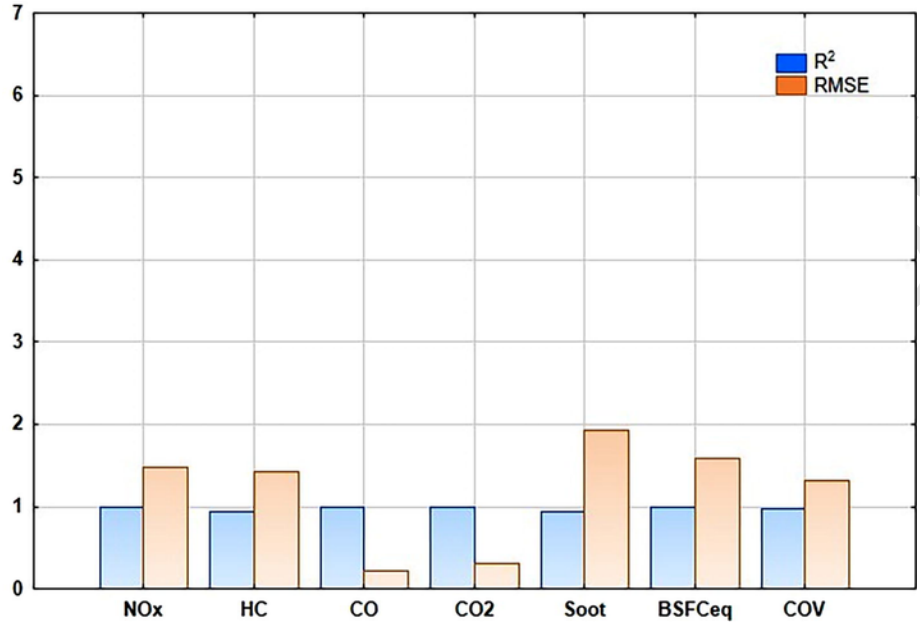

Fig. 16. Comparison of the correlation coefficient metrics for 8 neurons.

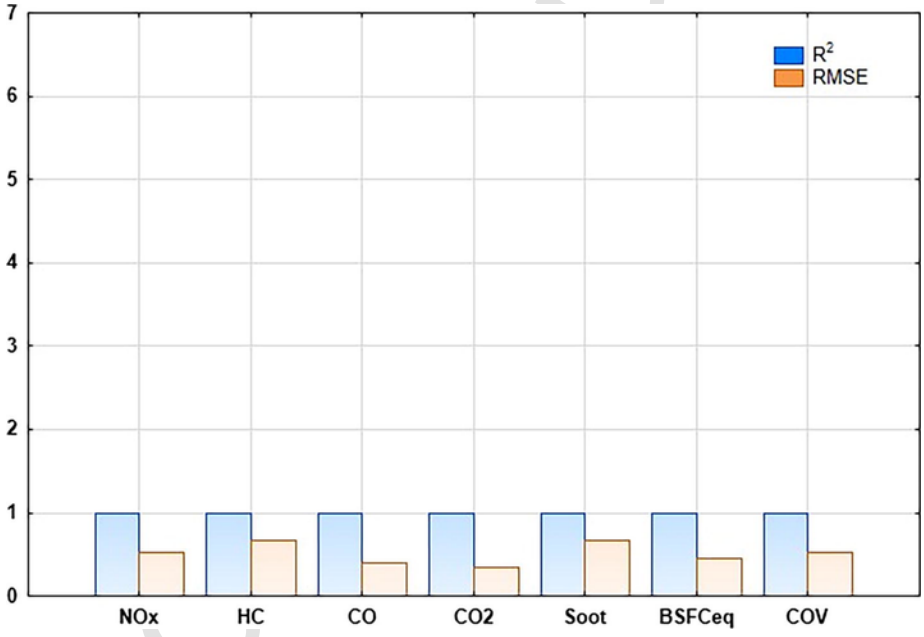

Fig. 17. Comparison of the correlation coefficient metrics for 10 neurons.

injection duration, the hydrous percentage was not considered as a separate input variable for the modelling endeavour. Considering the necessity to sustain a credible index of generalization capability of the desired ANN model it was deemed pivotal that the data set array presented to the ANN solver was kept uniform across the input variables such that random partitioning of the input data set into training and validation subsets prior to the solver run would not be skewed or biased by an input variable with inconsistent or missing observations. Hydrous methanol strategies uniquely by subsuming its effect within the input variable of methanol flow rate. Thus, as no separate input variable of water percentage addition was included as an input variable, training and validation data set consistency was preserved across all the chosen input variables uniformly across all load cases to maintain model generalization capability in the present ANN endeavour. Thus, owing to the prudence in the choice of the input variables, any scope of model over-fitting or loss of generalization for the 50% and 100% load cases was avoided. Prior to the present case of study, the correlation between selected input and output variables are verified through the correlation matrix in the Fig. 8 from which the contradictory influences of chosen inputs on the selected emission and performance parameters have been encapsulated. The correlation between the inputs and outputs has been evaluated in terms of the prevalent Pearson Product Moment correlation coefficient metric in line with the study of [33].

3.2. Model overfitting: considerations

As outlined in Section 1.1, one of the major challenges in ANN modeling is to avoid overfitting. Once the network is trained to predict its desired output with minimal error, then the network is expected to

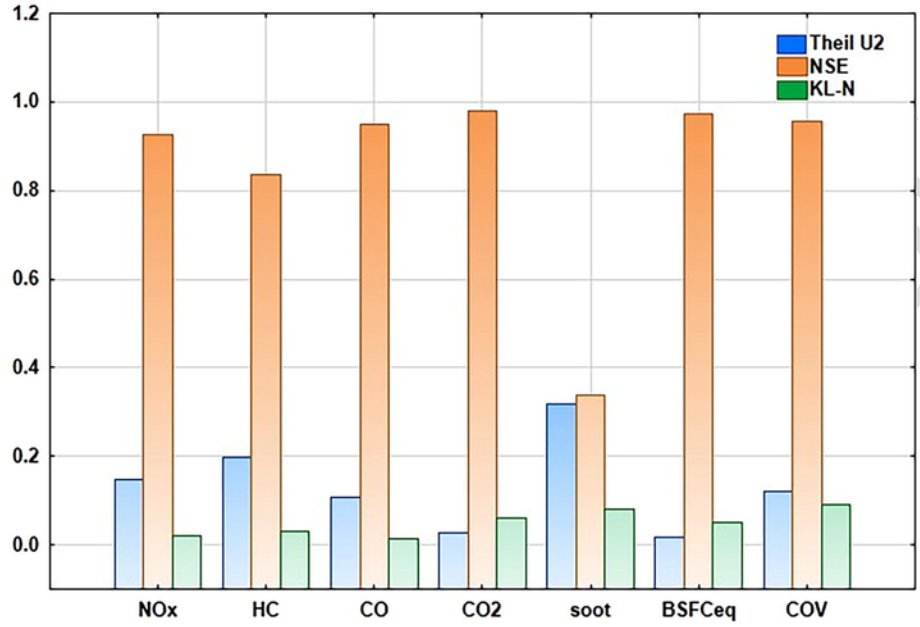

Fig. 18. Comparison of the Theil U2, NSE and KL-N for 6 neurons.

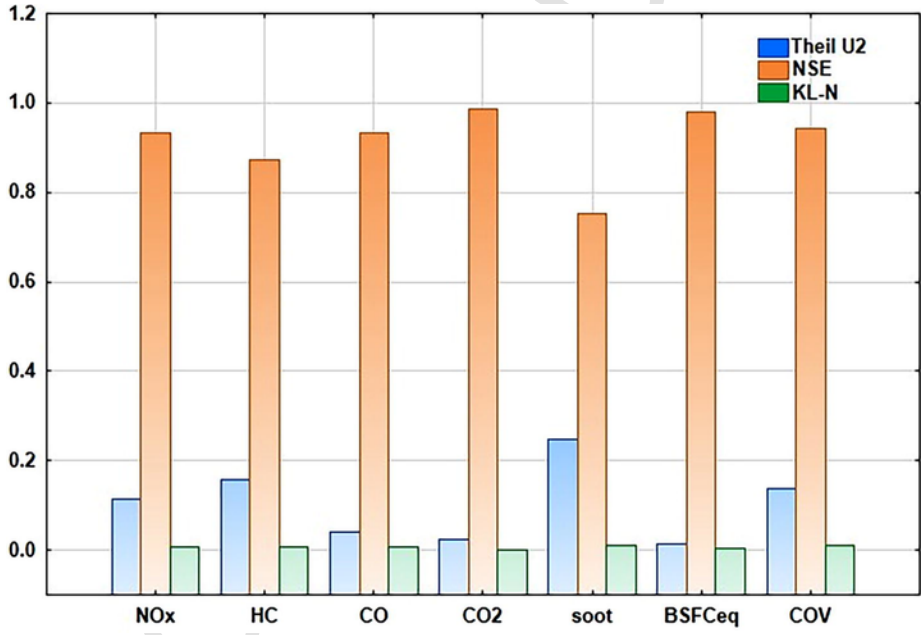

Fig. 19. Comparison of the Theil U2, NSE and KL-N for 8 neurons.

predict well for new sets of data also. But sometimes it predicts new patterns with higher degree of errors which eventually resulting in overfitting of data. It occurs as a result of inability of trained network to generalize the new data. Selection of appropriate number of hidden nodes has a significant role in circumventing the overfitting of data. Hecht-Nelson et al. had suggested the upper limit of the hidden neurons in their work [45] according to the Kolmogorov's theorem as $n_h \leq 2n_i + 1$, where n_i and n_h are the number of inputs and hidden neurons respectively. Considering this upper bound for present study, the number of maximum possible hidden neurons is computed as $2 \times 7 + 1 = 15$. Whereas another formula was proposed by Belman-Flores et al. [46] for the maximum limit of the hidden neurons of a system with single hidden layer in which the number of training sets were constrained by the formula-

$$n_T \geqslant c[n_h(n_i + 1)] \tag{3}$$

Therefore, according to Belman-Flores et al. [46] the upper limit of the number of hidden neurons is expressed as-

$$n_h \leqslant \left[\frac{n_T - cn_0}{c(n_i + n_0 + 1)}\right] \tag{4}$$

where c is the coefficient greater than or equal to 4 and n_o is the number of outputs. For this present study, the number of neurons can be calculated as-

$$n_h \leqslant \left[\frac{647 - 4 \times 7}{4(7 + 7 + 1)}\right] = \frac{619}{60} = 10.3 \approx 10 \tag{5}$$

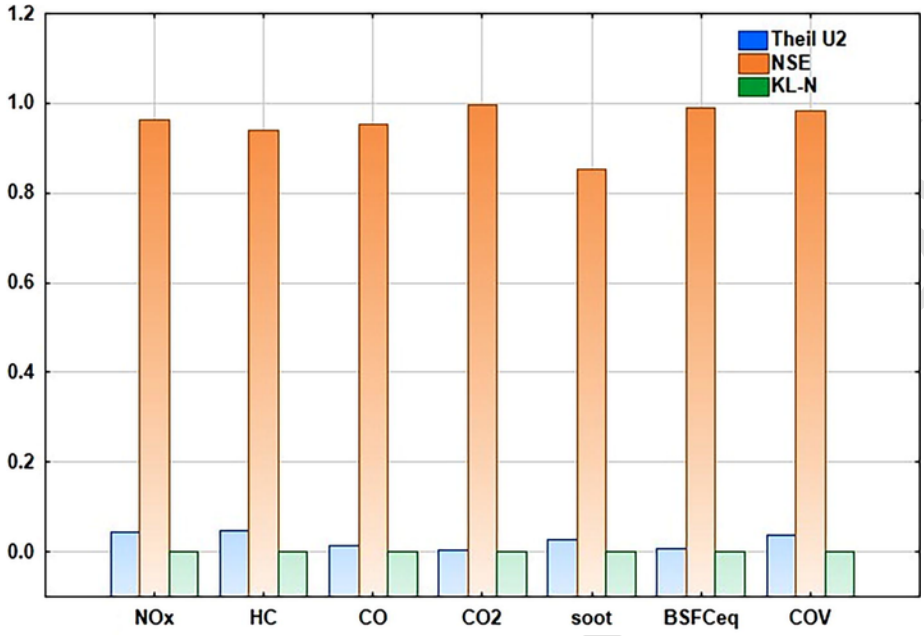

Fig. 20. Comparison of the Theil U2, NSE and KL-N for 10 neurons.

Table8
Total uncertainty of predicted values of GEP model.

Parameters	Uncertainties involved (Instrumental, Theil U2)	Calculations	Total uncertainty, U_T (%)
NOx	0.2 (<500 ppm vol), 0.045145	$\sqrt{(0.2)^2 + (0.045145)^2}$	0.20
	0.9 (≥500 ppm vol), 0.045145	$\sqrt{(0.9)^2 + (0.045145)^2}$	0.90
HC	0.1 (<200 ppm vol), 0.047117	$\sqrt{(0.1)^2 + (0.047117)^2}$	0.11
	0.2 (≥200 ppm vol), 0.047117	$\sqrt{(0.2)^2 + (0.047117)^2}$	0.20
CO	0.2 (<0.6% vol), 0.01414	$\sqrt{(0.2)^2 + (0.01414)^2}$	0.20
	0.3 (≥0.6% vol), 0.01414	$\sqrt{(0.3)^2 + (0.01414)^2}$	0.30
CO2	0.15 (<10% vol), 0.004149	$\sqrt{(0.15)^2 + (0.004149)^2}$	0.15
	0.2 (≥10% vol), 0.004149	$\sqrt{(0.2)^2 + (0.004149)^2}$	0.2
COV_{IMEP}	1.005, 0.036981	$\sqrt{(1.005)^2 + (0.036981)^2}$	1
soot	1, 0.026993	$\sqrt{(1)^2 + (0.026993)^2}$	1
BSFCeq	1.82, 0.007375	$\sqrt{(1.82)^2 + (0.007375)^2}$	1.82

In this present case of study total 924 data sets are available out of which 70% of total sampling (647) has been utilized as training sets which is far away from the minimum value of training sets as described by the Eq. (6).

$$n_T \geqslant 4 \times [15 \times (7 + 1)] = 480 \quad (6)$$

However, the lower value of neurons computed from Hecht-Nelson et al. ($n_h = 15$) and Belman-Flores et al. ($n_h = 10$) was considered as the maximum number of neurons according to the work of Amir et al. [47] in a system with single hidden layer. Consequently, for this study 10 numbers of hidden neurons were considered as the upper limit beyond which overfitting may occur.

3.3. Solver architecture: choice and selection

In this study, the selection of optimum neurons in the hidden layer has been made based on an empirical procedure. The number of neurons has been selected as 6, 8 and 10 which is the maximum number of neurons to avoid overfitting as discussed in the Section 3.2. Different statistical error metrics of model evaluation for 6, 8 and 10 neurons has been shown in the Figs. (9–20). From the Figs. (9–20), it has been noticed that the model for 6 neurons is having the capability to predict BSFCeq with significant accuracy while accuracy in predicting NOx is not acceptable. As depicted in Figs. (9–20), the best number of neurons in the model to predict BSFCeq is found to be 6 neurons whereas to predict NOx it is found to be 10 neurons. However, in this study the variation in prediction accuracy is minimized as the number of neurons increases. From the figures, it is observed that the value of MAPE is found below 5% only for 10 neurons which is considered to be the limiting value [33]. Furthermore, the RMSE of the model for 10 neurons has demonstrated very low values for all the outputs simultaneously. In multiple-input single-output (MISO) model there is the liberty to choose different number of neurons for each output while it increases the weights in the network. Whereas in multiple input multiple output models it is desired to predict simultaneously all the outputs with greater accuracy. Therefore, from the above discussion, it can be concluded that the optimum selection of neurons is considered to be 10 as the model is capable of predicting the outputs with high accuracy altogether. Selected network parameters for the proposed network have been tabulated in Table 7.

3.4. Model evaluation metrics

In view of the limitations of the widely used model evaluation metrics outlined in Sec 1.1, the present study undertakes a comprehensive evaluation of model credibility by subjecting the developed model to various error metrics invariant to scale transformation [19] along with uncertainty estimation measures to rationalize the robustness of the ANN model developed. Though the prevalent model evaluation metrics have been utilized for a benchmark of model performance in comparison to similar studies, each result from such metric has been further rationalized with respect to values obtained from a correspondingly scaled variation of the original metric to address its inherent limitations but retains the attribute of the conventional measure. Thus, the correlation metric of Nash-Sutcliffe Coefficient of Efficiency (NSCE) Eq. (8) has been used as a true estimator of model correlation with a view

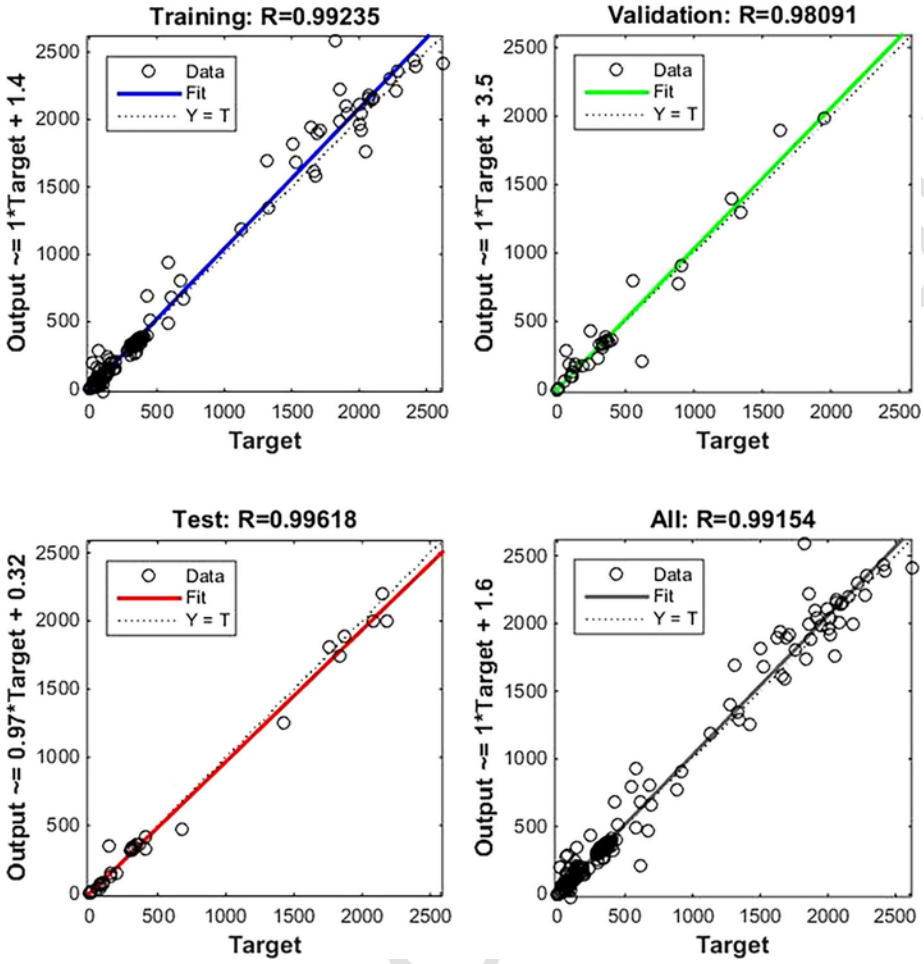

Fig. 21. Correlation coefficients of the developed network.

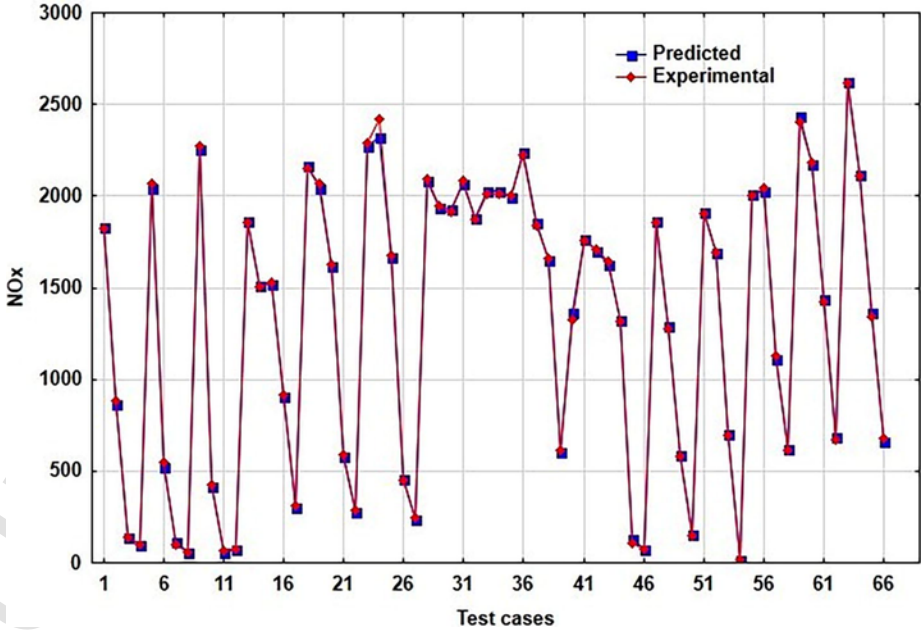

Fig. 22. Comparison of predicted NOx data with measured data.

to avoid overestimation of the degree of correlation indicated by values obtained by the ubiquitousR^2metric Eq. (7), which has been observed [41] to be limited by its inherent sensitivity to the means and variances

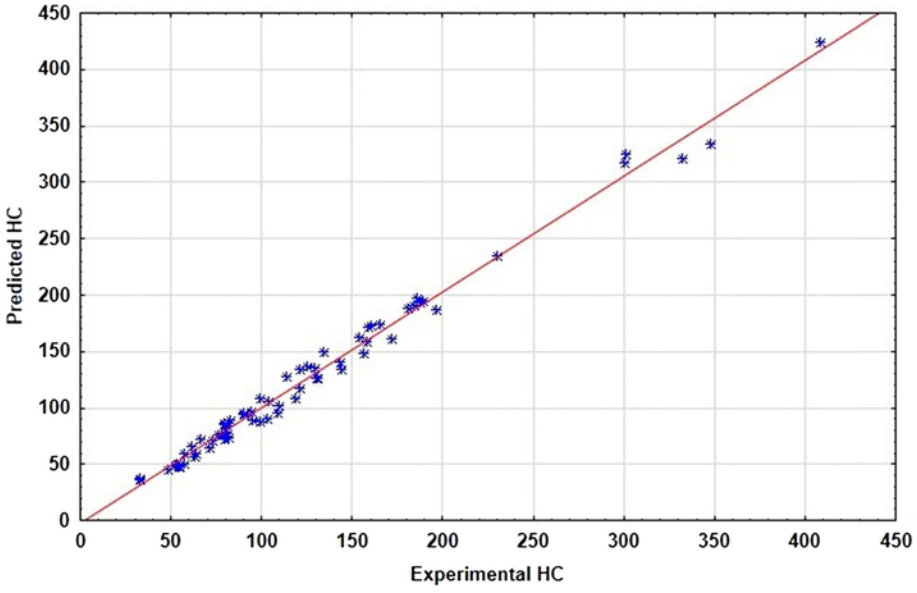

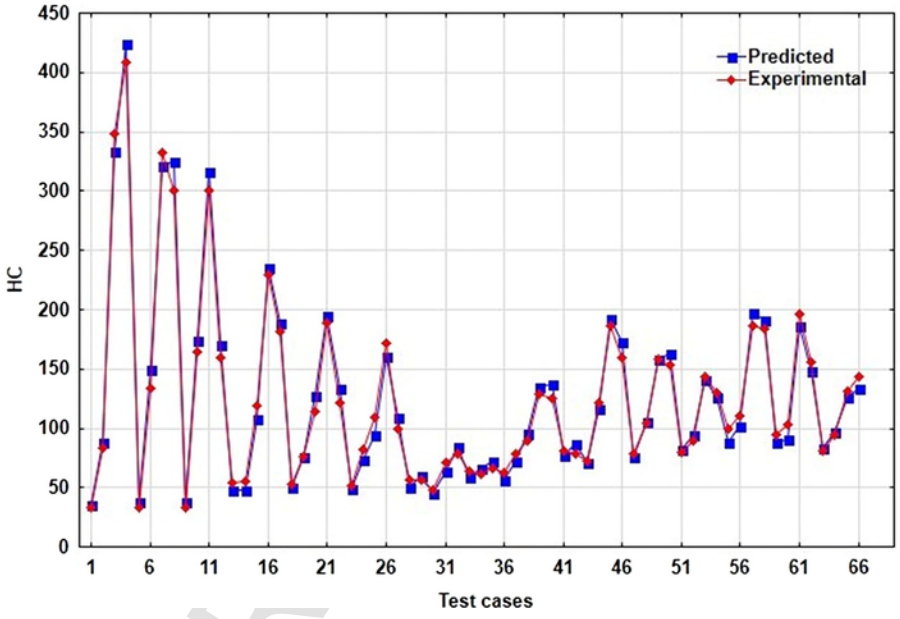

Fig. 23. Comparison of predicted HC data with measured data.

of the predicted and observed values.

$$R^2 = 1 - \left(\frac{\sum_{i=1}^{n} (t_i - o_i)^2}{\sum_{i=1}^{n} (o_i)^2} \right) \tag{7}$$

$$NSCE = \left[1 - \left\{ \frac{\sum_{i=1}^{n} (t_i - o_i)^2}{\sum_{i=1}^{n} (t_i - \hat{t})^2} \right\} \right] \tag{8}$$

Similarly, Symmetric mean absolute percentage error (sMAPE) Eq. (10) as proposed by Armstrong [48] has been employed as an absolute error measure in the present study to address the singularity issues of the common metric of Mean absolute percentage error (MAPE) Eq. (9) arising out of division by zero situations leading to bias in forecast accuracy of the data at the extremes of a range.

$$MAPE = \frac{1}{n} \sum_{i=1}^{n} \left(\left| \frac{t_i - o_i}{t_i} \right| \right) \times 100 \tag{9}$$

$$sMAPE = \frac{1}{n} \sum_{i=1}^{n} \frac{2 \times |t_i - o_i|}{|t_i| + |o_i|} \tag{10}$$

In addition to these model evaluation error metrics, Root mean square error (RMSE) Eq. (11) and normalized mean square error (NMSE) Eq. (12) have been employed in this study which are often preferred to MSE as MSE is more susceptible to the outliers' due to its added weights to larger errors. However, to diminish the scale dependency of RMSE, Normalized root mean square error (NRMSE) Eq. (13) has been employed which provides the comparison between different data sets with different scales whose lower value demonstrates smaller residual variation. Further, mean square relative error (MSRE) has been used in this study Eq. (14) as additional measure of scale independent metric which defines the sensitivity of the model towards higher

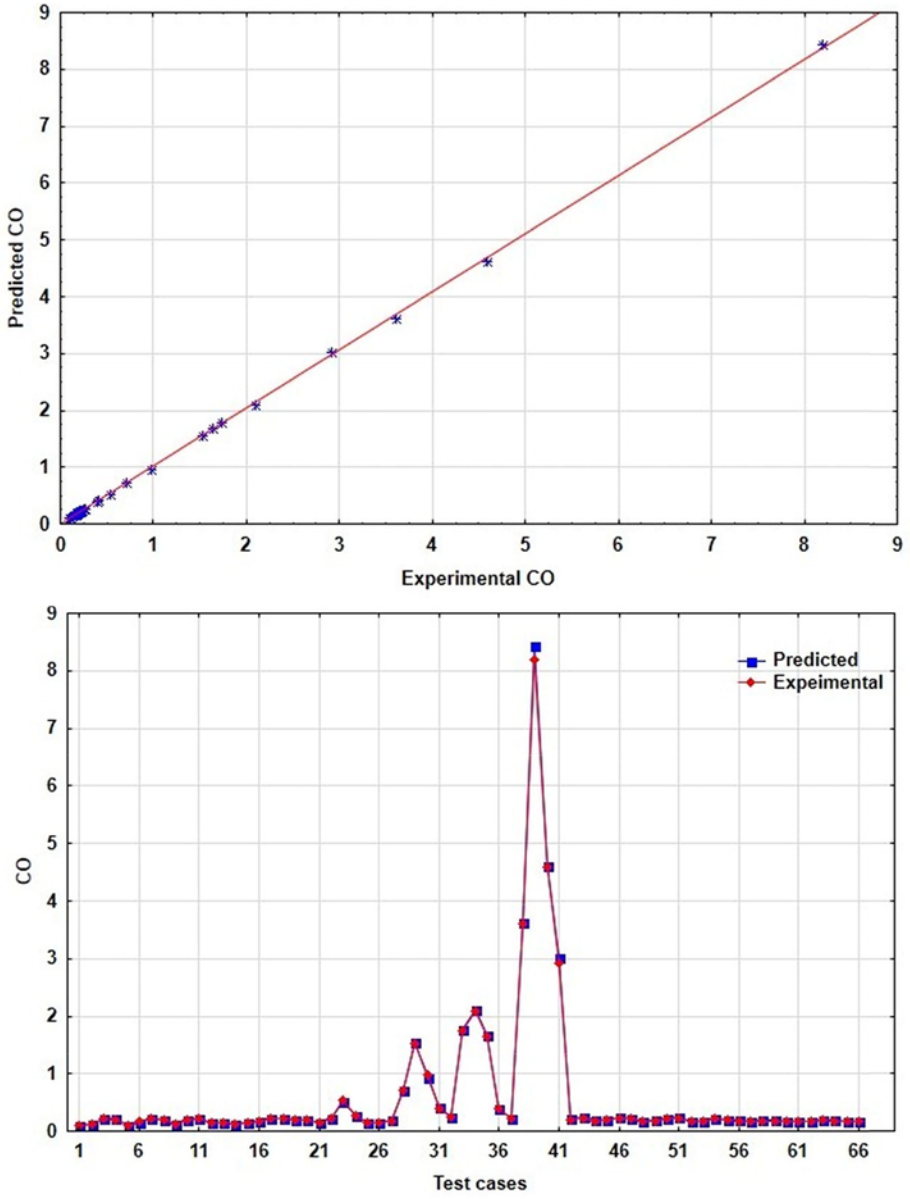

Fig. 24. Comparison of predicted CO data with measured data.

relative errors that occurs usually at lower values of estimation [12].

$$RMSE = \sqrt{\frac{1}{n}\sum_{i=1}^{n}(t_i - o_i)^2} \tag{11}$$

$$NMSE = \frac{1}{n}\sum_{i=1}^{n}\frac{(t_i - o_i)^2}{(\bar{t}) \times (\bar{o})} \tag{12}$$

$$NRMSE = \frac{\sqrt{\frac{1}{n}\sum_{i=1}^{n}(t_i - o_i)^2}}{t_{\max} - t_{\min}} \tag{13}$$

$$MSRE = \left|\frac{1}{n}\sum_{i=1}^{n}\left(\frac{t_i - o_i}{t_i}\right)^2\right| \tag{14}$$

where t_i is the observed value and o_i is the predicted value and n is the numbers of samplings in data set and $\bar{t}$ and $\bar{o}$ are the average of target and observed values respectively.

The Theil uncertainty metric commonly known as U2 proposed by Theil [49] is a measure of prediction quality of a developed model. In conjunction with the similarity in theme of the work of Banerjee et al. [12], Theil uncertainty was employed in this present study to measure the forecasting strength of the model. It gives a standardized measure which combines the mean error and the variance of errors of the predicted and observed values. Lesser value of Theil uncertainty signifies greater forecasting quality of the model.

$$U2_{THEIL} = \left[\frac{\sqrt{\sum_{i=1}^{n}(t_i - o_i)^2}}{\sqrt{\sum_{i=1}^{n}t_i^2}}\right] \tag{15}$$

KL-N matric model [50] based on Kullback-Leibler (KL) divergence was employed in this present study for evaluating the model accuracy. This evaluation metric includes the quadratic loss function leveled with corresponding variance of errors. It is measured as a distance between the true probability and arbitrary probability distribution in the course of probability theory and information theory. In this present study, ex-

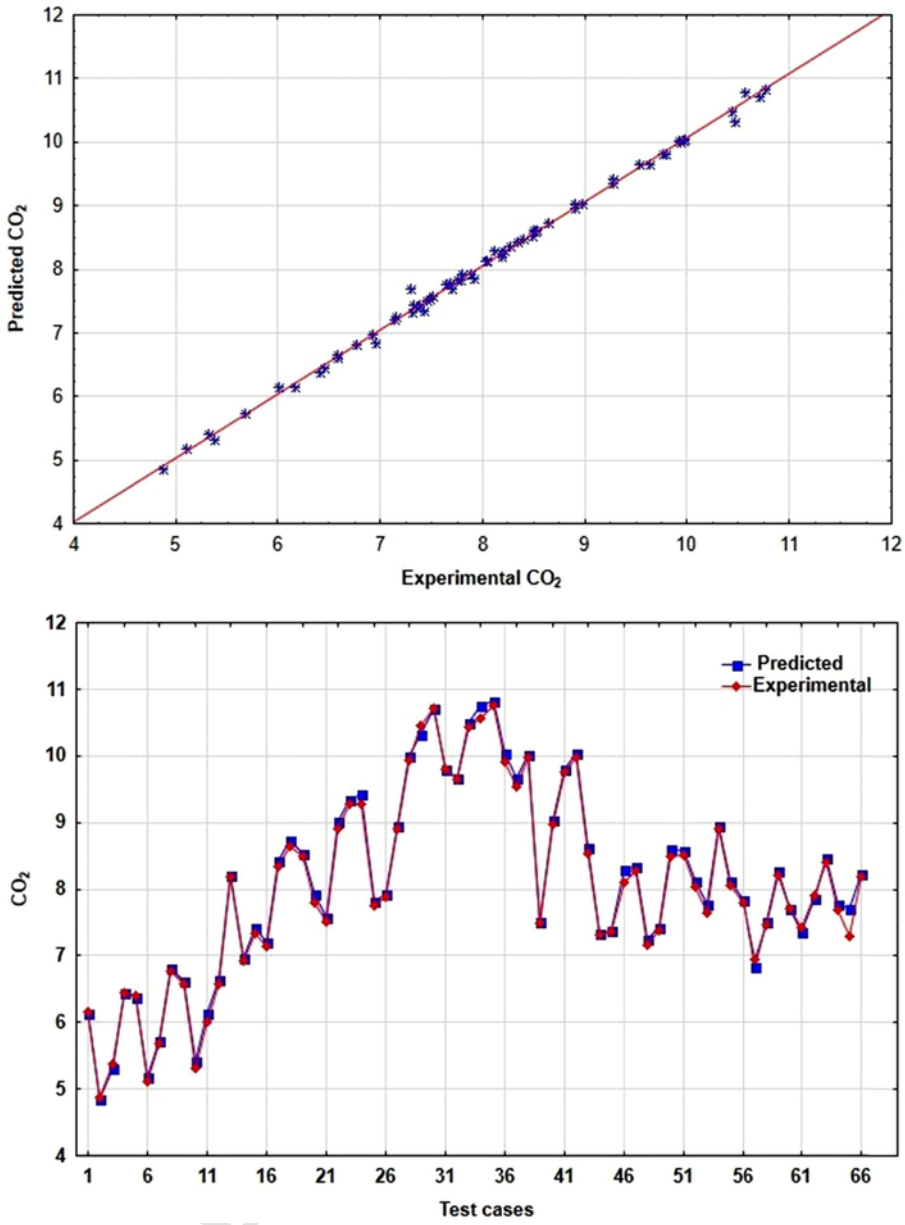

Fig. 25. Comparison of predicted CO_2 data with measured data.

perimental data were treated as the true probability distribution which is desired to be simulated by the model and the observed values were treated as arbitrary probability distribution. Kullback-Leibler (KL) divergence estimation provides a credible evaluative measure to estimate the capability of the model to generalize the new concealed data. Lower value of divergence shows higher generalization ability of the model presenting higher quality index of estimation.

$$KL - N_j = \sqrt{\frac{1}{n}\sum_{i=1}^{n}\frac{(p_i - t_i)_j^2}{(S_{AM}^2)_j}} \tag{16}$$

4. Results and discussion

The proposed ANN model was developed considering BP, FIP, EGT, % O2 (exhaust), diesel SFC, methanol SFC and Air flow rate as decision variables due to their characteristic ability to be sensed in real time. The ANN platform was tasked to emulate the engine performance-emission and stability parameters of BSFCeq, NOx, HC, CO, CO2, Soot and COVIMEP simultaneously. Section 4.1 outlays the experimental analysis of the PFI injected methanol-diesel PPCI dual fuel operation. The developed ANN model has been comprehensively cross-validated against the corresponding experimental markers in Section 4.2 and rationalized through the statistical metrics proposed in the Section 3.4.

4.1. Experimental paradigm

BSFCeq is one of the most important performance parameters in dual fuel engine in which SFC of multiple fuels are considered and expressed in one common platform. As apparent from Figs. S1–S6 there is a nature of increasing BSFCeq for all scope of experimentation compared to pure diesel operation. It has been found that the highest BSFCeq is occurred at 50% load and 500 bar injection pressure with methanol injection duration of 8 ms which is around 14% higher compared to baseline diesel operation. The lowest BSFCeq has been noted

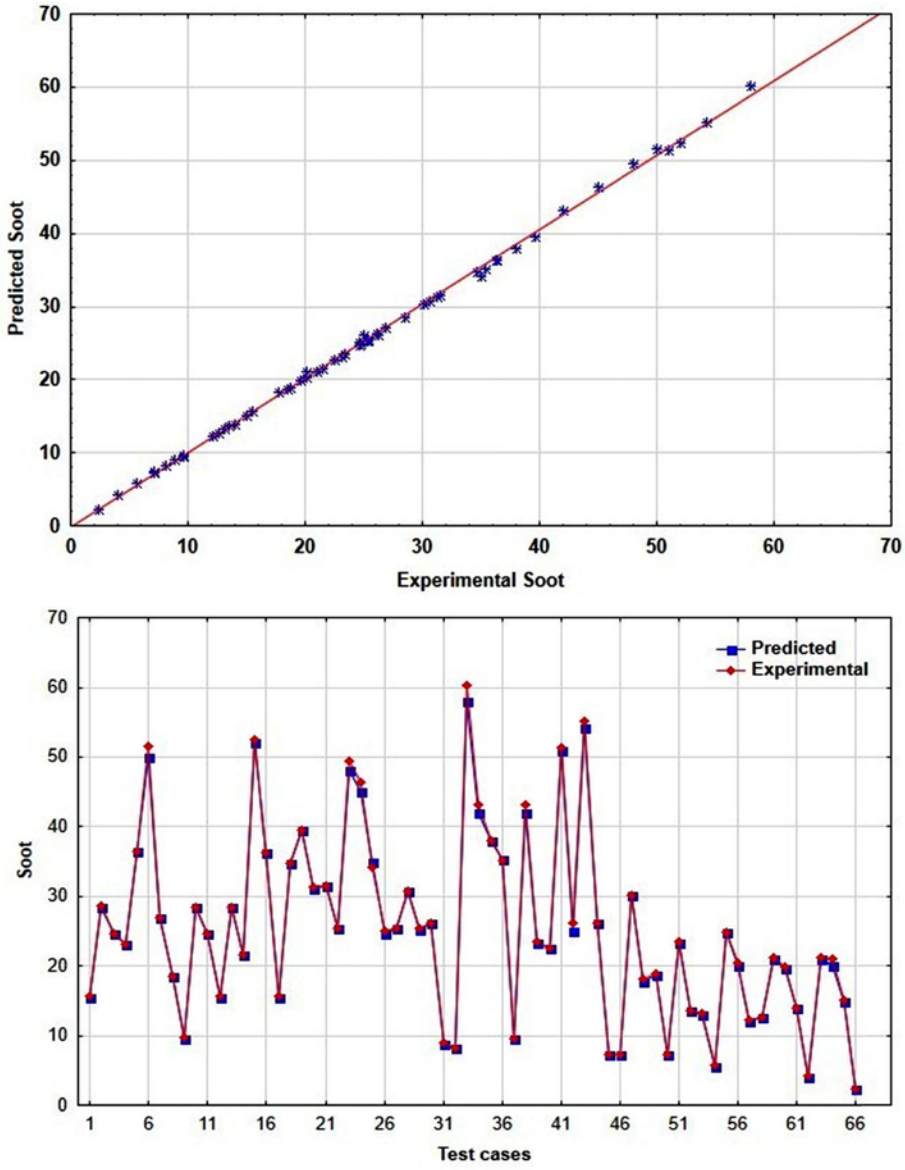

Fig. 26. Comparison of predicted soot data with measured data.

at 50% load and 600 bar injection pressure at baseline diesel operation. In case of hydrous methanol addition, the highest value of BSFCeq is recorded at 500 bar injection pressure with 10% hydrous methanol addition for 10 ms injection duration which is 31% higher than the baseline diesel operation. Therefore, it can be concluded that for methanol-diesel dual fuel operation, BSFCeq has an increasing trend compared to baseline diesel operation. BSFCeq is calculated using the following formula (Eq. *(17)*).

$$(BSFC_{eq})_{diesel} = \frac{\left[diesel_{SFC} + methanol_{SFC} \times \frac{(LHV)_{methanol}}{(LHV)_{diesel}}\right] \times 1000}{BP} \quad (17)$$

As evident from the Figs. S7–S12 the NOx emissions showed a decreasing trend for all methanol injection strategies except at full load conditions. Introduction of methanol in the regime of diesel combustion have significantly diminished the NOx emissions [51]. At 50% load, the maximum reduction of 97% of NOx was achieved compared to baseline diesel at 400 bar through the injection of 0.63 kg/hr methanol for 8 ms injection duration whereas at 500 and 600 bar, 94.5% and 96.8% reductions were achieved respectively. Similarly, for 75% load, NOx reduction showed the same trend as amount of NOx depletes in faster rate with the addition of methanol. Maximum 86.3%, 83.3% and 89.2% reductions were achieved respectively at 400, 500 and 600 bar fuel injection pressure when compared to baseline diesel. However full load condition did not follow the same trend in NOx emission reductions. Unlike 50% and 75% load, full load exhibits only 10% and 8% improvement in NOx emissions at 400 and 500 bar correspondingly but at 600 bar NOx initially decreased by 63.2% and then suddenly increased to 5% and 30% with further addition of methanol. Injection of hydrated methanol further decreased the NOx emissions upto 99.3% at 600 bar compared to baseline diesel and improves the situation additionally by 10.1% comparing with anhydrous methanol while developing same power. This lowering of NOx was resulted from the cooling nature of the methanol owing to higher latent heat of vaporization which compressed the peak in-cylinder temperature in diesel-methanol dual fuel combustion paradigm.

From Figs. S13–S18 it is revealed that the emissions of unburnt HC exhibit increasing nature for the entire experimental endeavor in this study irrespective to load, FIP and methanol injection quantity. Only higher percentage of methanol shows some decreasing nature at all

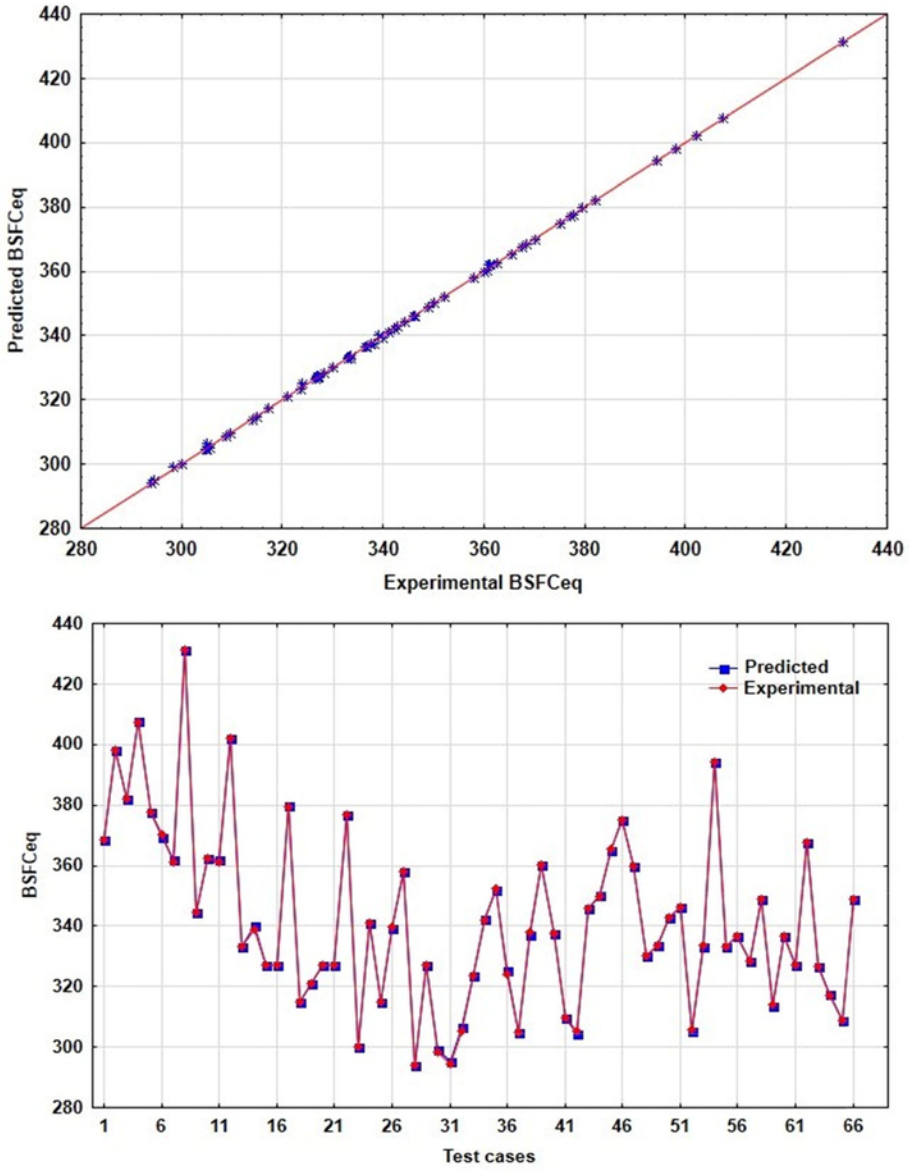

Fig. 27. Comparison of predicted BSFCeq data with measured data.

FIPs. At 50% load, unburnt HC shows increasing trend for all conditions at 400 bar whereas at 75% load, initially unburnt HC emission increases with methanol addition but at 10 ms injection duration the amount of unburnt HC decreases. However, at full load condition, no significant effect on unburnt HC emissions is observed for all scope of experimental conditions. At 500 and 600 bar methanol addition of 8 ms and 10 ms injection duration at 50% and 75% load respectively shows a decreasing trend. For hydrated methanol addition, the situation improves slightly wherein only 10 ms injection duration of methanol shows a decreasing nature of unburnt HC emission. At low load conditions, unburnt HC emission is exceptionally higher whereas maximum reduction of unburnt HC of 15% for anhydrous methanol is found at full load condition. For anhydrous methanol addition, maximum amount of 408 ppm of HC has been observed at 50% load whereas 230 ppm of maximum amount has been found at 400 bar in case of hydrated methanol addition. The higher level of unburnt HC is possibly resulted from the lower in-cylinder temperature owing to addition of methanol. Therefore, it can be summarized that the methanol like high octane fuel addition to diesel always demonstrates a higher level of unburnt HC emissions.

From the Figs. S19–S24, it is encapsulated that in case of 50% and 75% load, injection of methanol shows very less effects on emissions of CO whereas at full load conditions significant changes in CO emissions have been observed with the addition of methanol. At full load condition, methanol injection for 4 ms injection duration at all FIPs, demonstrates an immense NSCE increase in CO emissions, but with further injection of methanol, CO emissions decreased to a very low level compared to baseline diesel. Maximum reduction in CO emissions compared to baseline operation has been found as 94.25% at highest load with methanol injection for 10 ms at 600 bar. While in case of hydrated methanol injection, uneven effects have been observed on CO emissions. At 400 bar FIP in case of hydrated methanol case compared to anhydrous one, CO emissions increases initially but it shows a decreasing trend with further gradual increment in methanol addition whereas at 500 bar, CO emissions decreases at first and then starts increasing with higher methanol injection rate. On the contrary, at 600 bar for each strategy of hydrous methanol injection for all load conditions, a massive reduction in CO emissions compared to diesel only mode has been noticed as shown in Fig. S24. A maximum level of 71.24% reduction in CO emission has been achieved at 600 bar in anhydrous case in

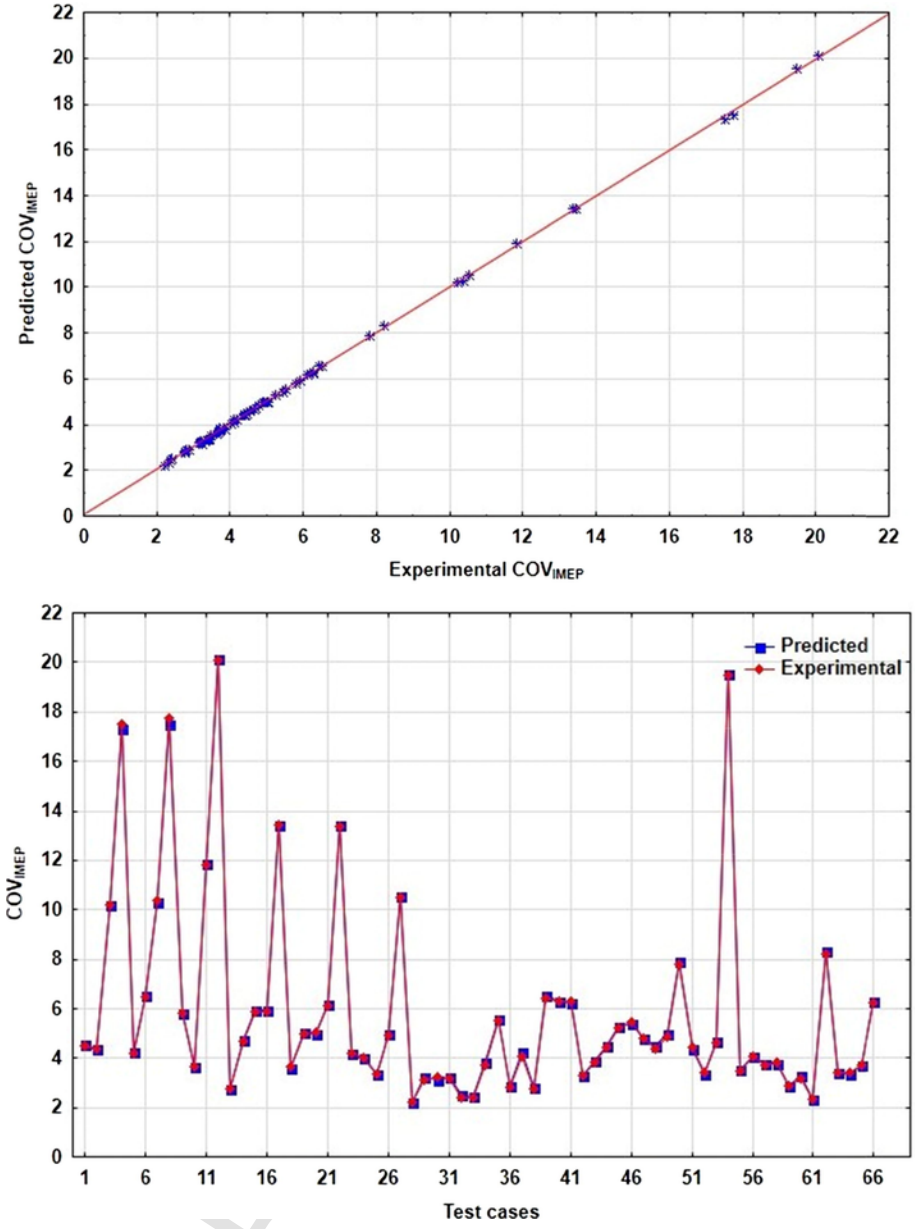

Fig. 28. Comparison of predicted COV_{IMEP} data with measured data.

combination with the hydrous methanol injection case. Therefore, it can be concluded that CO emissions have a decreasing trend with respect to methanol addition at full load conditions whereas for hydrous methanol injection of all strategies have shown a massive decreasing trend at 600 bar.

From the Figs. S25–S30 it can be summarized that the methanol injection rate has an insignificant effect on the emissions of CO_2. Though at higher loads, CO_2 emission has increased but effect of FIP is still found to be negligible. The maximum CO_2 level of 10.77% has reached at 75% load with 500 bar of FIP at a methanol injection rate of 0.4552 kg/hr for 6 ms injection duration. Whereas the minimum value is found to be 4.88% at 50% load with 400 bar of FIP for 4 ms methanol injection duration at a rate of 0.274564 kg/hr. Similarly, injection of hydrous methanol is also showing the same trend as that of anhydrous methanol. By summarizing from the Figs. S25–S30, it can be concluded that the emission of CO_2 is highly dependent on load only, whereas it is rarely sensitive to any other parametric variations.

In this study COV_{IMEP} is used as a stability index of combustion which defines the range of operation for lower load conditions. Figs. S31–S33 revealed that the injection of methanol have increased the coefficient of variance (COV) of IMEP raising the possibility of misfire. As depicted in the Figs. S31–S33, the highest methanol injection rate was restricted due to misfire occurring at each FIP for 50% load. At 75% load, similar trend of increasing COV_{IMEP} was observed as summarized from Figs. S31–S33. At 100% load, no significant effects of methanol injection rate on COV_{IMEP} were noticed. However hydrated methanol injection as depicted in Figs. S34–S36 has also shown the same nature of increasing COV_{IMEP} at all FIPs even at 100% load. Therefore, it can be concluded that the methanol addition can affect the stability of the dual fuel engine by raising the chance of misfire which limits its injection rate especially at lower loads.

As depicted in Figs. S37–S39 the emission of soot is showing a decreasing trend with the injection of methanol. Though at lower load the effect of methanol injection is not so significant, but the overall soot emission is decreased as the amount of methanol injection in-

creases. The lowest level of soot emission is found to be 8.16 mg/m^3at full load for 10 ms injection duration which is nearly 74% lower when compared with the baseline diesel. Moreover, injection of hydrous methanol as apparent from Figs. S40–S42 helps in further decreasing in soot emission while the lowest value is found to be 2.37 mg/m^3 which is 95% lower when compared to baseline operation. Therefore, it can be concluded that the injection of hydrous as well as anhydrous methanol facilitates the reduction of soot emission for all conditions of operations.

4.2. Artificial neural network modelling evaluation

The ANN model has been developed considering the inputs as BP, FIP, diesel flow rate, methanol flow rate, air flow rate output oxygen and EGT which was acquired from the experimental results to predict the output results as NOx, HC, CO, CO_2, soot and BSFCeq COV_{IMEP}. The forecasting ability of the model for the engine response in this study has shown a good agreement with the correlation statistics. However, the total uncertainty associated with model prediction is the consequence of two different aspects. One is the Theil uncertainty which is considered in ANN model development whereas the other one is associated with the experimental instrumentations. The total uncertainty in model prediction is demonstrated in Table 8.

As observed from the Figs. (21–28), the predicted values are commendably concurrent with the actual observation for the whole engine operation. This implies that the robustness of the prediction model to estimate performance, emissions and combustion parameters simultaneously with outstanding precision irrespective of the case of the engine operation.

The comparison of predicted values vs. experimental values for BSFCeq has been shown in the Fig. 27. The predicted values exhibit an extremely low MSRE of 0.001131 with Theil uncertainty of 0.007375 as well as KL-N estimation of 0.002. NMSE and NRMSE for BSFCeq were found as 0.000344 and 0.007115. Additionally, Nash-Sutcliffe Efficiency (NSCE) has also displayed excellent agreement with the experimental results which exhibits a value of 98%.

Fig. 22 have illustrated the statistical agreement of predicted values with the experimental results for NOx. It shows an exceptionally low Theil uncertainty of 0.045145 along with MSRE of 0.035671. Other statistical measures like NMSE, NRMSE have also demonstrated a very low magnitude. In special error metrics, NSCE was observed as high as 96% whereas KL-N estimation was found to be 0.0006which satisfied the superior agreement of predicted values with the experimental results. Statistical investigation of HC discovered that the developed model contained a very low MSRE value of 0.026493 with RMSE of 0.67589 and MAPE of 2.8% along with Theil uncertainty of 0.047 across all the test points. Similar trend was also observed for CO in which value of MSRE, NMSE, NRMSE were found to be 0.035796, 0.000941 and 1.53E-05 respectively as evident from Fig. 24. The Theil uncertainty was also observed to be as low as 0.01414 along with KL-N content of 0.0021. ANN predicted CO_2 showed the importunate concurrency with the observed experimental values as depicted in Fig. 25. It revealed the value of MSRE content as 0.001742 along with NMSE and NRMSE as 0.00089 and 0.001489 respectively. The Theil uncertainty for predicted CO_2 was also found to be very low as 0.004149 whereas NSCE efficiency was observed as high as 99.6%. In the same way, soot was predicted precisely by the ANN model which is encapsulated in the Fig. 26. The predicted values of soot by the developed model scored exceptionally low MSRE, NMSE and NRMSE of 0.041268, 0.0026 and 0.002196 respectively. The Theil uncertainty was observed as 0.026993 along with MAPE of 2.49% while KL-N estimation was found to be as low as 0.0007 Fig. 27.

The concurrency of predicted COV_{IMEP} by the developed model with observed COV_{IMEP} from experimentation was demonstrated in the Fig. 28. The value of MSRE, NMSE and NRMSE for COV_{IMEP} was observed as 0.035108, 0.007341 and 0.001544 respectively. The developed model scored NSCE efficiency as high as 0.98463 along with the Theil uncertainty as low as 0.036981. In addition, KL-N divergence content showed a very low value of 0.001which displayed its good accuracy in prediction.

5. Conclusions

In this study, an artificial intelligence-based system identification tool as ANN has been employed to predict the performance, emissions and combustion parameters of a PFI injected methanol-diesel dual fuel engine coupled with CRDI. Developed ANN model contains an input layer with 7 neurons, a single hidden layer with 10 neurons and an output layer with 7 neurons (7-10-7). The prediction characteristic with interpolation and extrapolation along with the robustness of the model has been evaluated on a statistical platform containing different errors and performance analysis. The error analysis revealed that the developed model predicted the experimental results with a very high degree of accuracy with the value of R^2 ranging from 0.99990 to 0.988187 along with NMSE varying from 0.021813 to 9.62E-05. The NSCE efficiency was found to be varied from 0.948306 to 0.9960669. Hence it can be concluded that the developed ANN model can efficiently emulate the on-board performance, emission as well as combustion (stability) characteristics of a methanol-diesel dual fuel mode in an efficient manner. Consequently, the present study has established the ANN model as a consistent, reliable and robust system identification tool for PFI injected methanol-diesel dual fuel mode of operation in contemporary IC engine *meta*-modeling control paradigm.

Conflict of interest

None.

Acknowledgement

The authors gratefully acknowledge the kind support of the AICTE (Govt. of India) grant under the RPS projects entitled ''An experimental study to explore the potential of biodiesel ethanol blend as an alternative fuel in diesel engine with hydrogen enrichment" under Grant No: 8023/BOR/RID/RPS(NER)-34/2010-11 and ''Development of an artificial intelligence model to simulate the performance and emission characteristics of a diesel engine operating in dual fuel mode with biodiesel and CNG under various EGR strategies" under Grant No: 8023/RID/RPS-4/508 (POLICYIII) (NER)/2011-12.

Appendix A. Supplementary data

Supplementary data to this article can be found online at https://doi.org/10.1016/j.enconman.2019.01.087.

References

[1] S. Khandal, et al., Paradigm shift from mechanical direct injection diesel engines to advanced injection strategies of diesel homogeneous charge compression ignition (HCCI) engines-A comprehensive review, Renew Sustain Energy Rev 70 (2017) 369–384.
[2] D. Kim, et al., In-cylinder CO and UHC imaging in a light-duty diesel engine during PPCI low-temperature combustion, SAE Int J Fuels Lubr 1 (1) (2009) 933–956.
[3] Fridriksson H, et al. CFD investigation of heat transfer in a diesel engine with diesel and PPC combustion modes. SAE Technical Paper. 2011.
[4] Kimura S, et al. New combustion concept for ultra-clean and high-efficiency small DI diesel engines. SAE Technical Paper. 1999.
[5] Y. Qian, et al., Experimental studies on combustion and emissions of RCCI fueled with n-heptane/alcohols fuels, Fuel 162 (2015) 239–250.
[6] B. Lawler, et al., Thermally stratified compression ignition: a new advanced low temperature combustion mode with load flexibility, Appl Energy 189 (2017) 122–132.

[7] H. Xie, et al., Study on spark assisted compression ignition (SACI) combustion with positive valve overlap at medium–high load, Appl Energy 101 (2013) 622–633.
[8] J. Liu, A. Yao, C. Yao, Effects of diesel injection pressure on the performance and emissions of a HD common-rail diesel engine fueled with diesel/methanol dual fuel, Fuel 140 (2015) 192–200.
[9] J. Li, W. Yang, D. Zhou, Review on the management of RCCI engines, Renew Sustain Energy Rev 69 (2017) 65–79.
[10] Y. He, C. Rutland, Application of artificial neural networks in engine modelling, Int J Engine Res 5 (4) (2004) 281–296.
[11] S. Roy, et al., Development of an ANN based system identification tool to estimate the performance-emission characteristics of a CRDI assisted CNG dual fuel diesel engine, J Nat Gas Sci Eng 21 (2014) 147–158.
[12] R. Banerjee, P. Bose, Development of a neuro genetic algorithm based virtual sensing platform for the simultaneous prediction of NOx, opacity and bsfc in a diesel engine operated in dual fuel mode with hydrogen under varying EGR conditions, SAE Int J Engines 5 (2) (2012) 119–140.
[13] X. Lu, et al., Effect of port fuel injection of methanol on the combustion characteristics and emissions of gas-to-liquid-fueled engines, Energy Fuels 23 (2) (2009) 719–724.
[14] Najafi G, Yusaf T. Experimental investigation of using methanol-diesel blended fuels in diesel engine. In: Proceedings of the 4th International Conference on Thermal Engineering Theory and Applications. 2009.
[15] Z. Chen, et al., The impact of methanol injecting position on cylinder-to-cylinder variation in a diesel methanol dual fuel engine, Fuel 191 (2017) 150–163.
[16] D.K. Soni, R. Gupta, Optimization of methanol powered diesel engine: a CFD approach, Appl Therm Eng 106 (2016) 390–398.
[17] Atkinson CM, Long TW, Hanzevack EL. Virtual sensing: a neural network-based intelligent performance and emissions prediction system for on-board diagnostics and engine control. SAE Technical Paper. 1998.
[18] R. Isermann, J. Schaffnit, S. Sinsel, Hardware-in-the-loop simulation for the design and testing of engine-control systems, Control Eng Pract 7 (5) (1999) 643–653.
[19] C. Chen, J. Twycross, J.M. Garibaldi, A new accuracy measure based on bounded relative error for time series forecasting, PLoS One 12 (3) (2017), e0174202.
[20] C. Sayin, et al., Performance and exhaust emissions of a gasoline engine using artificial neural network, Appl Therm Eng 27 (1) (2007) 46–54.
[21] S. Walters, M. De Zoysa, R. Howlett, Monitoring the air–fuel ratio of internal combustion engines using a neural network, Meas Sci Technol 17 (10) (2006) 2773.
[22] M. Gölcü, et al., Artificial neural-network based modeling of variable valve-timing in a spark-ignition engine, Appl Energy 81 (2) (2005) 187–197.
[23] E. Arcaklioğlu, İ. Çelıkten, A diesel engine's performance and exhaust emissions, Appl Energy 80 (1) (2005) 11–22.
[24] A. de Lucas, et al., Modeling diesel particulate emissions with neural networks, Fuel 80 (4) (2001) 539–548.
[25] M. Canakci, et al., Prediction of performance and exhaust emissions of a diesel engine fueled with biodiesel produced from waste frying palm oil, Expert Syst Appl 36 (5) (2009) 9268–9280.
[26] H. Oğuz, I. Sarıtas, H.E. Baydan, Prediction of diesel engine performance using biofuels with artificial neural network, Expert Syst Appl 37 (9) (2010) 6579–6586.
[27] B. Ghobadian, et al., Diesel engine performance and exhaust emission analysis using waste cooking biodiesel fuel with an artificial neural network, Renew Energy 34 (4) (2009) 976–982.
[28] N. Hashemi, N.N. Clark, Artificial neural network as a predictive tool for emissions from heavy-duty diesel vehicles in Southern California, Int J Engine Res 8 (4) (2007) 321–336.
[29] P. Shayler, M. Goodman, T. Ma, The exploitation of neural networks in automotive engine management systems, Eng Appl Artif Intell 13 (2) (2000) 147–157.
[30] Papadimitriou I, et al. Neural network based fast-running engine models for control-oriented applications. SAE Technical Paper. 2005.
[31] A.A. Rai, et al., Comparison of modeling techniques to be used as an objective function in optimization techniques, IOP conference series: materials science and engineering, IOP Publishing, 2018.
[32] S.A. Kalogirou, Artificial intelligence for the modeling and control of combustion processes: a review, Prog Energy Combust Sci 29 (6) (2003) 515–566.
[33] S. Roy, R. Banerjee, P.K. Bose, Performance and exhaust emissions prediction of a CRDI assisted single cylinder diesel engine coupled with EGR using artificial neural network, Appl Energy 119 (2014) 330–340.
[34] A. Chakraborty, S. Roy, R. Banerjee, An experimental based ANN approach in mapping performance-emission characteristics of a diesel engine operating in dual-fuel mode with LPG, J Nat Gas Sci Eng 28 (2016) 15–30.
[35] C.W. Dawson, R.J. Abrahart, L.M. See, HydroTest: a web-based toolbox of evaluation metrics for the standardised assessment of hydrological forecasts, Environ Modell Software 22 (7) (2007) 1034–1052.
[36] J.S. Armstrong, R. Fildes, Correspondence on the selection of error measures for comparisons among forecasting methods, J Forecast 14 (1) (1995) 67–71.
[37] C. Yao, et al., Combustion Stability Control of Dieseline PPCI Based on In-Cylinder Pressure Signals, IFAC-PapersOnLine 49 (11) (2016) 333–339.
[38] B. Mohan, et al., Optimization of biodiesel fueled engine to meet emission standards through varying nozzle opening pressure and static injection timing, Appl Energy 130 (2014) 450–457.
[39] P. Devan, N. Mahalakshmi, Performance, emission and combustion characteristics of poon oil and its diesel blends in a DI diesel engine, Fuel 88 (5) (2009) 861–867.
[40] C.M. Noor, et al., Application of artificial neural network for prediction of marine diesel engine performance, IOP conference series: materials science and engineering, IOP Publishing, 2015.
[41] M.A. Yassin, A.A. Alazba, M.A. Mattar, Artificial neural networks versus gene expression programming for estimating reference evapotranspiration in arid climate, Agric Water Manage 163 (2016) 110–124.
[42] A. Menon, et al., Characterization of a class of sigmoid functions with applications to neural networks, Neural Networks 9 (5) (1996) 819–835.
[43] T. Al-Shemmeri, S. Oberweis, Correlation of the NOx emission and exhaust gas temperature for biodiesel, Appl Therm Eng 31 (10) (2011) 1682–1688.
[44] S. Wang, et al., Effect of air-excess on blends of RON70 partially premixed combustion, Flow Turbulence Combust 96 (2) (2016) 309–326.
[45] Hecht-Nielsen R. Kolmogorov's mapping neural network existence theorem. In: Proceedings of the IEEE International Conference on Neural Networks III. IEEE Press. 1987.
[46] J.M. Belman-Flores, et al., Analysis of a variable speed vapor compression system using artificial neural networks, Expert Syst Appl 40 (11) (2013) 4362–4369.
[47] A.H. Gandomi, D.A. Roke, Assessment of artificial neural network and genetic programming as predictive tools, Adv Eng Softw 88 (2015) 63–72.
[48] J.S. Armstrong, Long-range forecasting, Wiley, New York ETC, 1985.
[49] C.M. Kshirsagar, R. Anand, Artificial neural network applied forecast on a parametric study of Calophyllum inophyllum methyl ester-diesel engine out responses, Appl Energy 189 (2017) 555–567.
[50] Chen Z, Yang Y. Assessing forecast accuracy measures. Preprint Series, 2004. 2010: p. 2004–10.
[51] K. Anand, R. Sharma, P.S. Mehta, Experimental investigations on combustion, performance and emissions characteristics of neat karanji biodiesel and its methanol blend in a diesel engine, Biomass Bioenergy 35 (1) (2011) 533–541.